NATIONAL TRANSPORTATION SAFETY BOARD

Office of Research and Engineering
Materials Laboratory Division
Washington, D.C. 20594

March 12, 2018

MATERIALS LABORATORY FACTUAL REPORT Report No. 18-017

A. ACCIDENT INFORMATION

Place	:	Amherst, South Dakota
Date	:	November 16, 2017
Vehicle	:	TransCanada Keystone pipeline
NTSB No.	:	PLD18LR001
Investigator	:	Kalu Kelly Emeaba, RPH-20

B. COMPONENTS EXAMINED

Section of pipeline and piece of concrete set-on pipeline weight.

C. DETAILS OF THE EXAMINATION

Overall views of the submitted components are shown in figures 1 and 2. The pipe section was approximately 9 feet 10 inches long and contained a rupture extending up to approximately 4 feet 4 inches long in the axial direction. At its widest point, the rupture opening was 11.25 inches wide. Unlabeled brackets in figure 1 indicate a portion of the fracture with flat fracture features perpendicular to the wall and curving crack-front arrest lines, features consistent with fatigue as described in the next subsection of this report.

The pipe segment had been installed in a marshy area, and concrete set-on weights had been installed over the pipe at approximately 20-foot intervals to prevent the pipe from rising to the surface. A set-on weight had been located at the upstream end of the submitted pipe piece at the location indicated in figure 1, and a piece of that set-on weight was included for examination as shown in figure 2. More details about the set-on weight piece are provided in the last subsection of this report.

1. Pipe Piece

The ruptured segment of pipe was a 30-inch diameter pipe with a nominal wall thickness of 0.386 inch and a double submerged arc welded (DSAW) longitudinal seam. The pipe had been manufactured in 2008 by Berg Steel Pipe Corporation, located in Panama City, Florida. The steel pipe was certified to American Petroleum Institute (API) Specification 5L Grade X70 product specification level (PSL) 2 with a fusion-bonded epoxy (FBE) coating. The maximum operating pressure for the pipeline was 1440 psig.

Closer views of the ruptured area of the pipe as received are shown in figure 3, and a view of the fracture surface at the origin area is shown in figure 4. The pipe section had been partly cleaned on scene, but deposits of oil and isolated chunks of oil-soaked soil remained adhered to the pipe surface. The fracture surfaces had also been cleaned using oil-dissolving solvents and a nylon brush. After cleaning, the fracture surfaces were sprayed with a light oil and then brush-coated with Tectyl 506[1]. During cutting operations to remove the pipe, a fire was extinguished, and fire extinguishing material appearing as a white powder covered much of the exterior and interior surfaces of the pipe as received.

A closer view of the left side[2] of the fracture is shown in figure 4. A region of the fracture surface bounded by the dashed lines in figure 4 was relatively smoother and was perpendicular to the pipe wall, consistent with fatigue crack growth. Ratchet marks[3] were observed on the fracture surface, and curving crack-front arrest lines were consistent with fatigue emanating from multiple origins near the exterior surface as indicated with a bracket in figure 4. Near the middle of the fatigue region, the fatigue region intersected the interior surface along a length of 1.95 inches as indicated in figure 4. The fatigue region measured up to 5.52 inches long, and the depth was up to the full wall thickness of 0.3921 inch as measured with a ball-flat micrometer near the origin area.

The longitudinal seam and circumferential welds were used as reference points throughout the examination. The top of the pipe had been marked with yellow and orange paint on scene and is referenced as the 12 o'clock position in figure 1. The longitudinal seam in the joint containing the fatigue region was located 6.5 inches clockwise[4] from the top of the pipe, or approximately the 1 o'clock position. The upstream end of the fatigue region was located 12.8 inches downstream from the girth weld, and the upstream end of the through-wall portion of the fatigue fracture was located 14.9 inches downstream from the girth weld. Relative to the longitudinal seam, the fracture along the length of the fatigue region was located 10.75 inches counterclockwise from the seam, or approximately the 11:30 clock position.

Areas of the exterior surface adjacent to the fracture surface had missing coating, and exposed metal surface areas were disturbed with sliding contact marks. The sliding contact marks were observed on both sides of the fracture as shown in figures 5 through 7 and were mostly aligned nearly parallel to the longitudinal axis of the pipe. On the counterclockwise side of the fracture shown in figure 5, the area of sliding contact marks extended up to 9 inches upstream of the girth weld and up to 21.5 inches downstream of the girth weld, including the surface adjacent to the fatigue region. The circumferential width of the sliding contact area measured up to 3.5 inches wide measuring counterclockwise from the fracture.

On the clockwise side of the fracture shown in figures 6 and 7, sliding contact marks were present in two separate areas. In the upstream area shown in figure 6, sliding

[1] Daubert Chemical Company, Chicago, Illinois.
[2] References to the left and right faces of the fracture are as viewed looking in the same direction as the flow direction with the fracture located at the upper side of the pipe.
[3] A ratchet mark is a small step in the fracture surface formed when two adjacent fatigue cracks originate on slightly offset planes.
[4] In this report, clock references will be as viewed looking in the same direction as the flow direction with the 12 o'clock position at the top of the pipe.

contact marks were located adjacent to the fracture surface including the fatigue region in an area between 2 inches to 21.75 inches from the girth weld and within 1.5 inches of the fracture surface. In a separate area located further clockwise from the fracture, sliding contact marks were observed between 16.5 inches and 36 inches from the girth weld. The area of contact marks was up to 6.5 inches wide starting 2.75 inches counterclockwise from the longitudinal seam, an area that included the 12 o'clock position. The upstream end of this region is shown in figure 6 adjacent to the coating blisters, and the downstream end is shown in figure 7.

Coating material was present intermixed with the sliding contact marks, and many edges of the remaining coating adjacent to individual contact marks were curled and rounded consistent with sliding contact deformation. Linear abrasions on the surface of intact coating was observed at the downstream end of the sliding contact marks as indicated with unlabeled arrows in figure 7. Blisters such as those indicated in figure 6 and flaking disbonded pieces of coating were observed at the edges of the sliding contact areas, consistent with expected FBE coating behavior at the edges of a holiday in the pipe protected by cathodic protection[5].

Next, a scalpel was used to collect samples of soil deposits, coating pieces, and deposits in the areas of sliding contact. Disbonded pieces of coating around the edges of the sliding contact areas were removed mostly by hand, but also with a wood tongue depressor or scalpel as needed. The coated areas of the pipe were then cleaned using Alconox and water and a brush or cloth to remove oil and soil from the surfaces. In the exposed areas of sliding contact where coating was missing or removed, mineral oil and acetone were used with a soft-bristle brush to remove oil deposits and the Tectyl 506 that had been applied on-scene. The work at this stage was completed in a minimally-heated high-bay area, so additional heat was applied with a heat gun as required to facilitate removal of the oil and Tectyl 506 deposits.

The cleaned surfaces were then scanned using a Faro EDGE FaroArm coordinate measurement device fitted with a Faro Laser Line Probe HD.[6] The 3-D point cloud data representing the exterior surface of the pipe was acquired and processed using Geomagic Studio 2014.[7] During data processing, the scanned edges were cropped to straight lines, and the reference axes were aligned such that the Z axis was parallel to the upward (vertical) direction and the X axis was parallel to the longitudinal axis of the pipe. The data was converted from a point cloud to polygons and exported as a 3D PDF, resulting in the interactive 3D PDF attached as Appendix A.

The coated areas of the cleaned pipe were inspected visually for evidence of bulging, disbondment, or separation in other areas away from the sliding contact marks

[5] Cathodic protection is a form of corrosion prevention accomplished by making the protected structure the cathode in an electrochemical cell. The FBE coating is nonconductive, and a holiday is a location where the coating is disturbed or weaker, thereby focusing current from the electrochemical process at the location of the holiday.
[6] FARO Technologies, Inc., Lake Mary, Florida.
[7] 3D Systems, Rock Hill, South Carolina

previously noted. One area of exposed metal was found on the longitudinal seam approximately 5 feet 9 inches from the girth weld as shown in figure 8. Blisters in the coating were observed surrounding the area of exposed metal as indicated. The remainder of the coating was smooth and intact with ink manufacturing marks visible on the surface and no evidence of disbondment.

Fluorescent magnetic particle inspection (MPI) was conducted on the pipe exterior in the areas of sliding contact where coating was missing or removed. The inspected surfaces were then photographed while illuminated with an ultraviolet light, and resulting images are shown in figures 9 through 11. Networks of crack indications and segments of linear indications were observed throughout the sliding contact marks both clockwise and counterclockwise from the fracture. Although many indications were observed, many of the indications could be associated with lips of overlapped metal and were not necessarily associated with cracks. Areas where indications appeared brighter and more linear were bracketed with a yellow wax marker and are visible in the sliding contact areas in figures 13 through 15.

After the MPI inspection was complete, longitudinal and shear wave ultrasonic testing was completed from the interior surface to inspect for cracks in the sliding contact areas. No relevant indications were noted during the shear wave inspection. Wall thickness outside the sliding contact areas was approximately 0.390 inch as measured with the ultrasonic gauge. Wall thickness measurements were noted as low as 0.339 inch in the areas of sliding contact.

Rectangular areas of the pipe including the rupture and a piece located opposite the longitudinal seam were marked for sectioning as shown on the cleaned pipe in figure 12. The pieces were then cut from the pipe using a plasma torch. Next, a handheld bandsaw was used to cut longitudinally to the upstream and downstream ends of the rupture, thereby separating the two sides of the fracture. In figures 13 and 14, the two sides of the fracture were photographed in close proximity showing the overall damage pattern in the area of sliding contact. A closer view of the sliding contact marks is shown in figure 15, where various marks are labeled for reference in this report. Many overlapping grooves were observed in the center portion of the contact area. However, some distinct grooves were apparent as labeled A through N.

Grooves A and B were oriented approximately parallel to each other and to the longitudinal axis of the pipe and extended the furthest upstream. Grooves A and B extended across the fracture with 2.5 inches of groove A and 0.4 inch of groove B located upstream of the rupture. The grooves were separated approximately 2 inches apart. The axial lengths of grooves A and B were 6.3 inches and 6.7 inches, respectively.

Grooves C and D were approximately parallel to each other and were oriented at a slight angle relative to the longitudinal axis. The marks were separated by approximately 0.45 inch. The length of these marks could not be determined due to other overlapping grooves.

Grooves E, F, G, H, I, and J were all approximately parallel to each other and to the longitudinal axis of the pipe. The grooves generally had a rounded shape at the bottom of the groove with finer longitudinally-oriented linear features consistent with sliding contact along the axial direction. Grooves E, H, and J were relatively deep with lips of raised metal at the sides of the grooves. The spacing between grooves E and H and between grooves H and J was approximately 1 inch. The spacing between adjacent grooves E and F and adjacent grooves G and H was the same at 0.43 inch. The spacing between grooves F and G was 0.18 inch. Grooves F, G, and H had an edge that appeared to be continuous along the length of the contact area. The lengths of grooves F, G, and H were approximately 11.8 inches, 11,5 inches, and 12.9 inches long. A continuous segment of groove E had a length of 7.5 inches between the girth weld and the downstream end of the groove, but similar grooves at that circumferential location extended up to 5.1 inches upstream of the girth weld. Continuity of grooves I and J could not be clearly established through the contact area, but the upstream end of a groove at approximately the same circumferential position as groove I was located approximately 10.6 inches from the downstream end of groove I.

Sliding contact marks K, L, and M were oriented at approximately 45 degrees to the longitudinal axis of the pipe. These marks interrupted the longitudinal grooves consistent with having been made after the other marks. Marks K and L were continuous across the two sides of the fracture and were approximately 1.5 inches apart. Marks L and M were nearly parallel and were approximately 1.25 inches apart where mark M intersected the fracture and were approximately 1.1 inches apart at the upstream end of mark L. Groove N had a change in direction with the downstream portion nearly parallel to the longitudinal axis and the upstream portion nearly parallel to contact mark M. The spacing between mark M and the parallel portion of groove N was 2.25 inches.

Next, the interior and exterior surfaces of the pieces shown in figure 13 were scanned with the Faro coordinate measurement device to obtain thickness profiles of the two sides. The scanned data was acquired in Geomagic Studio and was subsequently analyzed using the thickness plot tool in Geomagic Control X. Results showing thickness contours for the two pieces are shown in figures 16 and 17. The deepest grooves were located near the upstream end of groove L and the downstream end of groove H as shown in figure 16. Contact marks at the 12 o'clock position were relatively shallow as shown in figure 17. The depth of the groove at the origin area was not clear from the scan data due to the orientation of the fracture in the fatigue region and necking deformation in the overstress regions outside the fatigue region.

Wall thickness was measured in multiple locations using a ball-flat micrometer and a point micrometer as appropriate. Adjacent to the sliding marks near the girth weld, the wall thickness was 0.3947 inch measured using a ball-flat micrometer. Near the origin area, the wall thickness measured 0.3921 inch, also measured using a ball-flat micrometer. At the edge of sliding contact marks adjacent to the origin area on the left side of the fracture where a lip of deformed material was present, the thickness measured 0.400 inch on the peak of the lip using a ball-flat micrometer. At the right side of the fracture, wall thickness was measured using a point micrometer in the sliding contact mark approximately 0.25 inch from the fracture face along the length of the fatigue region, resulting in wall thickness measurements of 0.373 inch, 0.3725 inch, and 0.370 inch near the downstream end, middle, and upstream end of the fatigue region, respectively.

A piece of the pipe containing the fatigue region on the left side of the fracture and a portion of the sliding contact marks adjacent to the left side of the fracture was cut from the rest of the piece shown in figure 13 using a table bandsaw. Next, the piece was cleaned with a soft bristle brush using a solution of Alconox and water then rinsed with ethanol. The resulting cleaned piece is shown in figure 18.

Views of the cleaned fracture surface at the fatigue region are shown in figures 19 and 20. Red dashed lines in figures 19 and 20 indicate areas of the exterior surface adjacent to the fracture where sliding contact marks were observed. (Only a portion of the marks are visible in the view shown in figure 19.) Extending from the surface from multiple locations along the length of the sliding contact mark were a series of near-surface cracks. The near-surface cracks extended from the surface at a shallow angle up to the depth indicated by the yellow dashed line in figure 19. As shown in figure 19, the near-surface crack depth was greatest at the center of the fatigue region where the fatigue region extended to the interior surface. Fatigue features including ratchet marks and curving crack-front arrest marks emanated from the near-surface crack boundary.

Optical images of the fatigue region at higher magnification are shown in figures 21 and 22. The boundary for the near-surface cracks had discrete curved segments consistent with multiple individual cracks coalescing along most of the length of the fatigue region. Each discrete segment of the curving boundary was associated with multiple fatigue origins.

A magnified optical image of the middle portion of the fatigue region where the fatigue region extended to the interior surface of the pipe is shown in figure 23. For reference in this report, this portion of the fatigue region is referenced as origin area A as indicated in figure 21. At this location, the depth of the near-surface crack measured 0.098 inch. Eight relatively prominent crack-front arrest lines were observed as indicated with unlabeled arrows in figure 23. These arrest lines were generally characterized by a relatively large step or undulation at the crack front and crack reinitiation features such as emerging radial marks. The depths associated with the relatively prominent crack-front arrest lines were 0.166 inch, 0.189 inch, 0.222 inch, 0.246 inch, 0.257 inch, 0.267 inch, 0.300 inch, and 0.340 inch.

The piece shown in figure 18 was sectioned further to facilitate examination of the fatigue region using a scanning electron microscope (SEM). SEM images of the fracture surface at origin area A and the adjacent origin area upstream from origin area A are shown in figure 24. Each image in figure 24 is a montage of 12 individual SEM image that were stitched together to form an image of the fracture across the pipe wall thickness. The areas associated with the near-surface cracks are bounded with yellow dashed lines, and the extent of the fatigue region in the upstream origin area is indicated with a black dashed line in the right image. Unlabeled arrows indicate the general direction of fatigue crack propagation in each area.

A closer SEM view of fatigue origin area A is shown in figure 25. The near surface crack area had radial features consistent with fracture initiation at the exterior surface and propagation angled radially inward, circumferentially clockwise, and toward the downstream direction. Ratchet marks were present at the end of the near-surface crack between individual fatigue origin areas. Unlabeled arrows in figure 25 indicate several of the ratchet marks associated with origin area A.

An SEM view of typical features observed at higher magnification in the fatigue region are shown in figure 26. Transgranular fracture features consistent with fatigue were observed, but fine fracture features were mostly obliterated by post-fracture abrasion damage or were obscured by residual carbon-based deposits.

Next, the fracture surface was tilted to examine the fracture features associated with the near-surface cracks as directly viewed with the electron beam oriented approximately perpendicular to the fracture face. A view of one of the near-surface cracks at origin area A is shown in figure 27. The fracture surface had transgranular fracture features with river markings consistent with a cleavage or quasi-cleavage fracture features consistent with overstress fracture.

Areas beyond the fatigue region where fracture occurred on slant planes consistent with ductile overstress fracture were examined during the SEM examination of the fracture surface. Dimple features consistent with ductile overstress fracture were observed in these areas.

The piece shown in figure 18 was further sectioned using a water-cooled abrasive saw to facilitate metallographic examination of the pipe material in the area of sliding contact. A piece was also sectioned from an area where the coating was intact to examine the exterior surface in an area with an intact coating. The sectioned pieces from the sliding contact area are shown in figure 28. Three specimens labeled M1, M2, and M3 were mounted in plastic and prepared for examination. The labels in figure 28 point to the cut surface that was examined in each case. In mount M2, the section intersected a visible crack on the surface, and the downstream portion of the crack was later opened by lab fracture as indicated in figure 28.

Figure 29 shows the typical microstructure of the pipe material near the middle of the thickness as obtained from sample M3 etched with 4% nital etch (a solution containing 4% nitric acid in methanol commonly used for metallographic examination of steel). Near the surface in areas of sliding contact grooves, the microstructural features showed evidence of distorted grains and changes in microstructure as shown for mount M2 in figure 30. Some areas in all 3 mounts such as the area shown in figure 30 had a surface layer that etched differently from the underlying material and formed a distinct boundary between the surface layer and the underlying material. A bracket in figure 30 indicates the location of the surface layer, measuring up to approximately 0.001 inch thick at the location shown. The surface layers were only found in areas that were associated with sliding contact marks.

Next, mounted sample M2 was coated with a thin film of a gold/palladium alloy to avoid issues with charging of the nonconductive mount[8] during an SEM examination of the polished and etched sample. The surface layer was visible on the mounted cross-sections during the SEM examination, appearing smoother and somewhat lighter than the adjacent pipe material. Energy dispersive x-ray spectroscopy (EDS) was used to compare the composition of the surface layer to that of the underlying pipe metal, and typical results are shown in figure 31. The spectrum for the surface layer is shown in yellow in figure 31, and the spectrum for the pipeline steel is outlined in red. Both spectra showed a high peak of iron with smaller peaks associated with manganese and silicon consistent with a low-alloy steel. However, the spectrum for the surface layer showed a distinct peak for chromium that was mostly absent from the pipeline steel spectrum for respective areas analyzed under the same conditions. The upper and lower spectra shown in figure 31 are the same data, but the scale of the vertical axis was reduced in the lower image to highlight the smaller peaks. The chromium (Cr) peak is indicated in the lower spectrum where the difference in peak height between the surface layer (shown in yellow) and the underlying pipe metal (outlined in red) was evident. This difference in peak height for the chromium peak was consistently observed throughout the areas of sliding contact where surface layers were observed.

An EDS map[9] of the surface layer and adjacent pipe material was conducted on mount M2 in the area shown imaged in figure 32. The SEM image in figure 32 was obtained using the backscattered electron detector in composition mode,[10] and the surface layer in this view is indicated with an unlabeled bracket. Results for EDS mapping of the view shown in figure 32 are presented in figure 33 for each of the elements detected. Larger views of the maps for chromium and manganese are shown in figures 34 and 35, respectively, where distinct differences between the surface layer and the underlying pipe material were observed. Unlabeled brackets in figures 34 and 35 indicate the location of the surface layer. In the map for chromium shown in figure 34, the surface layer appeared slightly brighter, consistent with a higher concentration of chromium in that layer. In the map for manganese, the surface layer generally appeared slightly darker than the underlying pipe material, but several isolated bright areas consistent with higher concentrations of manganese were observed in the surface layer as indicated with unlabeled arrows in figure 35. Isolated bright spots in the manganese map were only observed in the surface layer and not in the underlying pipe material.

A series of images at the exterior surface of mount M1 were obtained using an optical metallograph and stitched together as shown in figure 36. Several near-surface

[8] Charging is the accumulation of negative charge on the surface that develops during electron imaging of nonconductive samples in a SEM under high vacuum and can result in distorted and overexposed images.
[9] EDS mapping provides a visual representation of the distribution of each detected element in the field of view. In the EDS map images, higher concentrations of the detected element appear brighter.
[10] SEM images produced using a backscattered electron detector in composition mode have contrast that is associated with atomic weight of the elements in the image. Areas with elements having higher atomic weights appear as a relatively lighter shade of gray compared to areas having elements with lower atomic weights.

cracks were observed at the surface in the area of sliding contact damage, and a closer view of one of the cracks is shown in figure 36. The crack profile had transgranular fracture features with a jagged crack path and a blunt tip.

Next, the polished and etched mount M1 was coated with a gold/palladium alloy for SEM and EDS analysis. SEM images using the backscattered electron detector of steel surface layers on the surface of M1 in the area of sliding contact are shown in figure 37. A bracket in the upper image indicates the thickness of the surface layer that appeared relatively smoother and brighter compared to the pipe material. A higher magnification view of the surface is shown in the lower image in figure 37, where overlapping layers of the surface deposit were observed. An EDS spectrum of the surface layer showing a small peak of chromium and a corresponding spectrum of the pipe material below the surface layer where the chromium peak was absent are shown in figure 38.

An optical metallograph image of the exterior surface of the mounted sample from an area with intact coating is shown in figure 39. The exterior surface was rough with no evidence of a deposited surface layer between the coating and the pipe surface. The mounted sample was coated with gold/palladium and examined with an SEM, and no evidence of a layer with a chromium peak was detected.

The piece of the pipe wall in the area of sliding contact between mounts M2 and M3 (see figure 28) was examined using the SEM. A crack-like feature was observed on the exterior surface as shown in figure 40. The fracture surface visible inside the crack opening is shown at higher magnification in the lower image in figure 40. Transgranular fracture features were observed with tear ridges, indicative of quasi-cleavage fracture features consistent with overstress fracture.

Areas of the exterior surface on the largest piece shown in figure 28 were also examined using the SEM and EDS. As the surface was examined, a difference in the EDS spectra was noted in areas within the sliding contact grooves versus undisturbed areas between the grooves. The examined area of sliding contact damage is shown in figure 41 before samples were taken for metallographic examination. Areas with relatively light gray and more reflective surfaces in the sliding contact marks are shown circled. In figure 42, a typical spectrum from an area with the lighter gray appearance (location A in figure 41) is shown. The EDS spectra in these areas contained a distinct peak of chromium consistent with the deposited steel layer observed in the metallographic mounts. By comparison, the chromium peak was largely absent from the surfaces between the sliding contact marks such as location B noted in figure 41 with the corresponding spectrum shown in figure 42.

The longitudinally-oriented sliding contact grooves generally had a rounded profile at the bottom of the grooves. The cut face for the piece upstream of mount M1 is shown in figure 43 where the groove profiles are visible. The radii of several of the grooves that were distinctly separate from overlapping damage were measured, and the measured grooves are labeled 1 through 5 in figure 43. An example of the measurement for groove

1 is shown in figure 44 where the radius of curvature measured approximately 0.233 inch. The radius of curvature for grooves 2 through 5 measured 0.116 inch, 0.103 inch, 0.085 inch, and 0.108 inch, respectively.

Hardness was measured on the cross-section of a piece cut from the pipe wall adjacent to mount M3. The average hardness from 3 indentations measured 95.5 HRBW. According to ASTM Standard A370,[11] the measured hardness in steel corresponds to a tensile strength of approximately 101,000 pounds per square inch.

A sample of the pipe wall cut from the side of the pipe opposite the longitudinal seam was sent to Lehigh Testing Laboratories in New Castle, Delaware, for mechanical testing and chemical analysis. Three room-temperature tensile tests were conducted using subsize round specimens with a ¼-inch diameter cross-section in the gage length and oriented in the transverse direction. Fifteen Charpy impact tests were conducted at 5 different temperatures ranging from -100°F to 212°F. The Charpy test specimens were subsize specimens with a 6.7-millimeter by 10-millimeter cross-section oriented in the transverse direction (notch pointing parallel to the longitudinal axis of the pipe).

Results of the mechanical testing and chemical analysis are presented in the test report included as Appendix B. The average yield strength, tensile strength, and elongation for the 3 tensile specimens were 87,700 pounds per square inch, 96,000 pounds per square inch, and 29 percent, respectively. In each of the 3 test specimens, the measured values for yield strength, tensile strength, and, elongation satisfied the requirements for steel manufactured to API 5L grade X70 PSL2 specifications.

The average Charpy impact energy at each of the tested temperatures was 110 pound feet, 93 pound feet, 81 pound feet, 74 pound feet, and 65 pound feet at 212°F, room temperature, 23°F, -50°F, and -100°F, respectively. The impact energy for each specimen at each of the temperatures including the lowest temperature exceeded the minimum average impact energy requirement for full-size Charpy impact test specimens tested at 32°F as listed in the API 5L specification for grade X70 PSL2 steel.[12]

Results of the chemical analysis for the pipe sample were within allowable ranges for carbon, manganese, phosphorus, sulfur, and titanium as listed in the API 5L specification for grade X70 PSL2 steel. Also, the combined totals for titanium, niobium, and vanadium were also within the allowable range included in the specification.

---

[11] ASTM International Standard A 370 – 12a, “Standard Test Methods and Definitions for Mechanical Testing of Steel Products,” *Annual Book of ASTM Standards*, ASTM International, West Conshohocken, Pennsylvania (2014).

[12] According to specification API 5L, the measured impact energy values for subsize specimens tested at 32°F or below are adjusted by dividing the measured value by the ratio of the actual specimen width to the full-size specimen width (0.67 in this case) to determine conformance with the full-size Charpy impact energy requirements listed in the specification.

2. Concrete Set-on Weight Piece

A schematic drawing of a concrete set-on weight installed on a pipeline is shown in figure 45. The weight had an upside-down U shape with the pipe running between the legs of the U. The interior faces of the weight were lined with an integral protective fibrous pad. The piece of the set-on weight that was received in the lab was the lower end of the left leg cut from the weight as indicated in figure 45.

The lower face of the set-on weight piece shown in figure 2 was mostly covered with oily dirt deposits, but a piece of the upstream end corner between the exterior face and the lower face was fractured away and appeared relatively clean consistent with a recent fracture. The set-on weight piece was cleaned using a solution of Alconox and water and acetone as needed with a soft-bristle brush and wood scrapers to remove oil and dirt deposits on the surface, and the resulting cleaned piece is shown in figures 46 and 47. During the cleaning process, chunks of the corner between the exterior face and the lower face were chipped away with a wood brush handle in the area indicated in figure 47.

Next, the weight piece was rotated onto its lower face to view the cut face. The cut face was then wetted with water to more clearly reveal the aggregate size and distribution, and a photograph of the wet cut face is shown in figure 48. The shapes of the aggregate were irregular, and the edges had varying radii of curvature in the plane of the cut. Approximate radius measurements at multiple locations around several of the pieces of aggregate are shown indicated in figure 48. Radii of curvature on the pieces ranged from a point with nearly zero radius up to a 0.65-inch radius.

Concrete samples from the corner between the cut face and the exterior face were chipped away near the upstream end of the weight piece. A hammer and steel chisel were required to chip the pieces away. A view of the weight piece after removing the samples is shown in figure 49, and several of the pieces chipped from the weight are shown in figure 50. The concrete samples were examined by a geologist at the Smithsonian Institution. Several of the larger pieces of aggregate within the samples were identified as quartzite and a mix of quartzite and feldspar as indicated in figure 50. Typical hardness values for quartzite and feldspar were higher than typical hardness of other aggregate pieces in the samples. The larger pieces that were identified as harder materials as indicated in figure 50 ranged from 1 inch or more across to less than ½ inch across. Smaller pieces of the harder rock are also scattered within the concrete matrix.

Matthew R. Fox, Ph.D.
Senior Materials Engineer

Adrienne V. Lamm
Materials Engineer

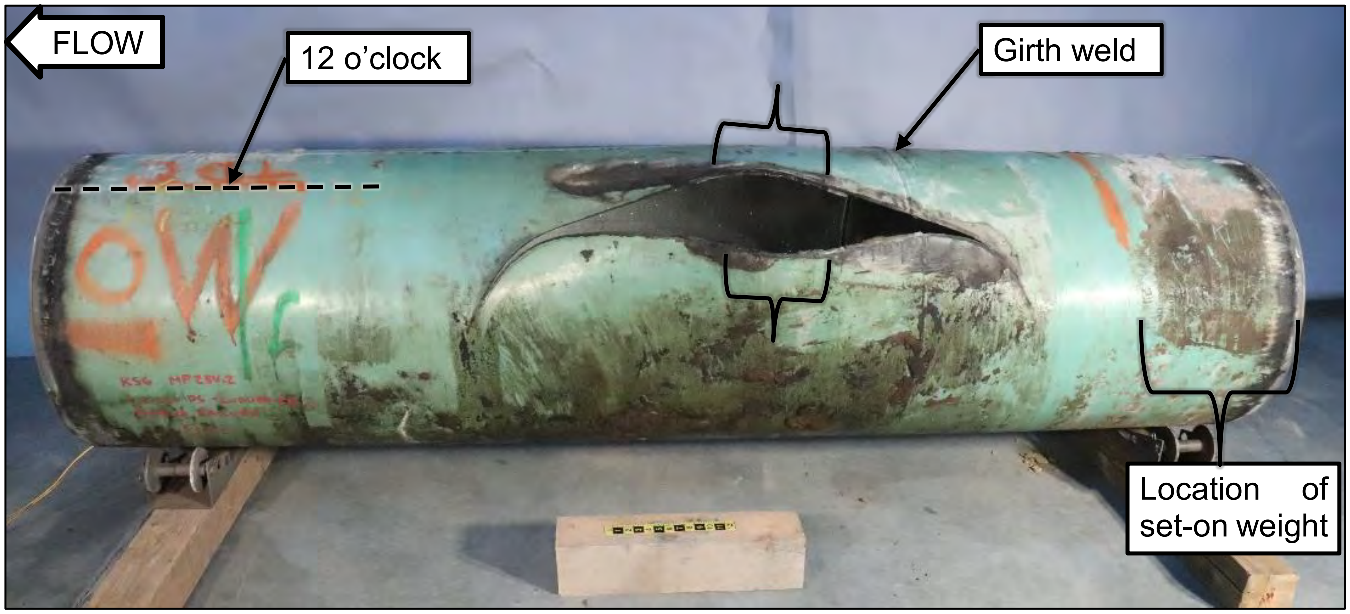

Figure 1. Overall view of the pipe piece. Unlabeled brackets indicate the location of fatigue features on the fracture surface.

Figure 2. Lower end of a concrete set-on weight leg submitted for examination with the pipe piece.

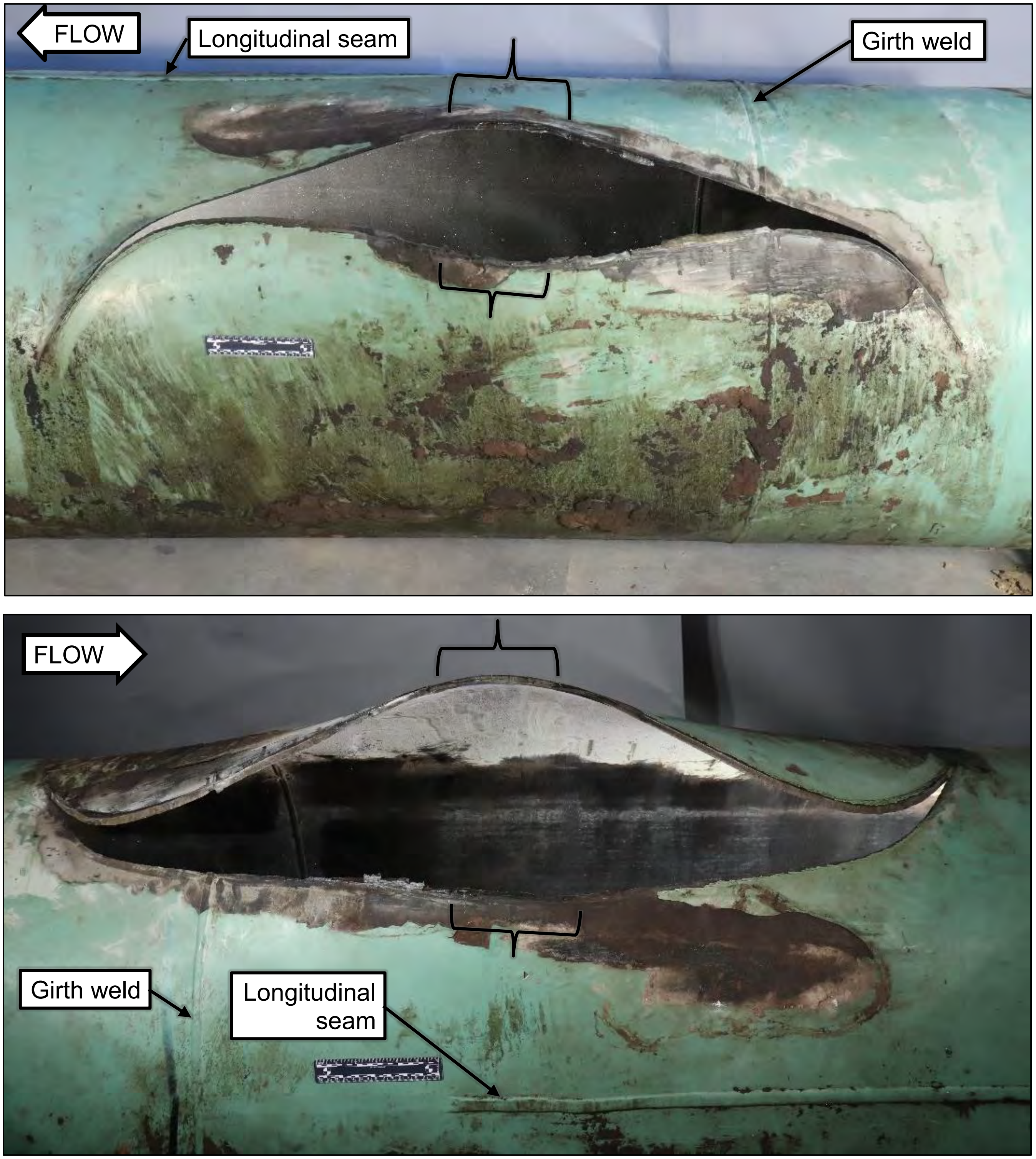

Figure 3. Overall views of the pipe rupture. Unlabeled brackets indicate the location of fatigue features on the fracture surface.

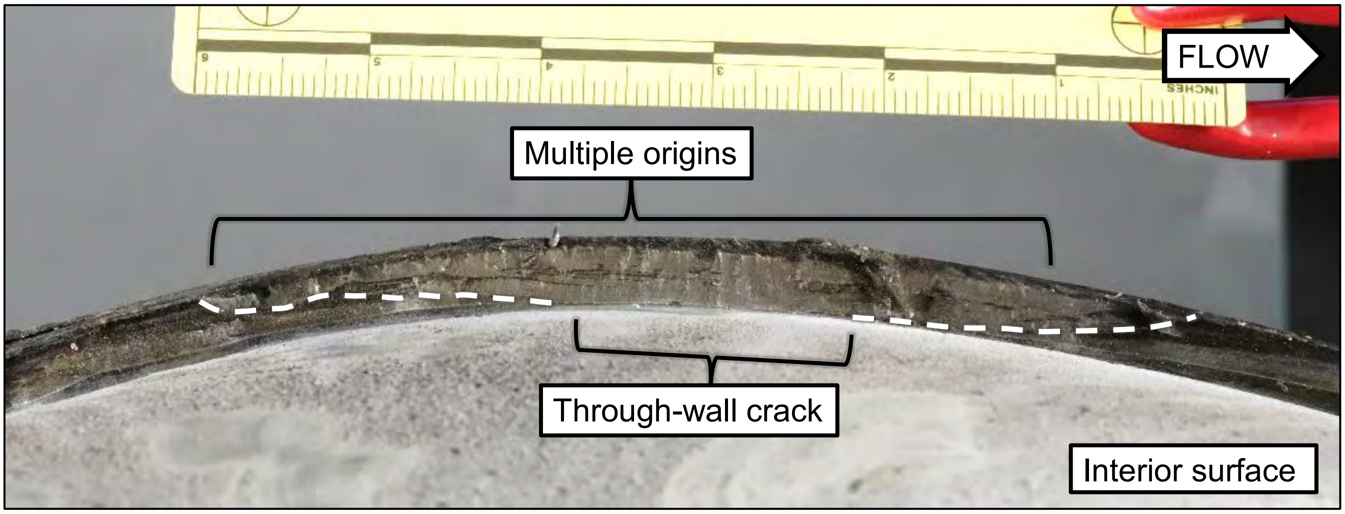

Figure 4. Closer view of the left side of the fracture showing the fatigue region.

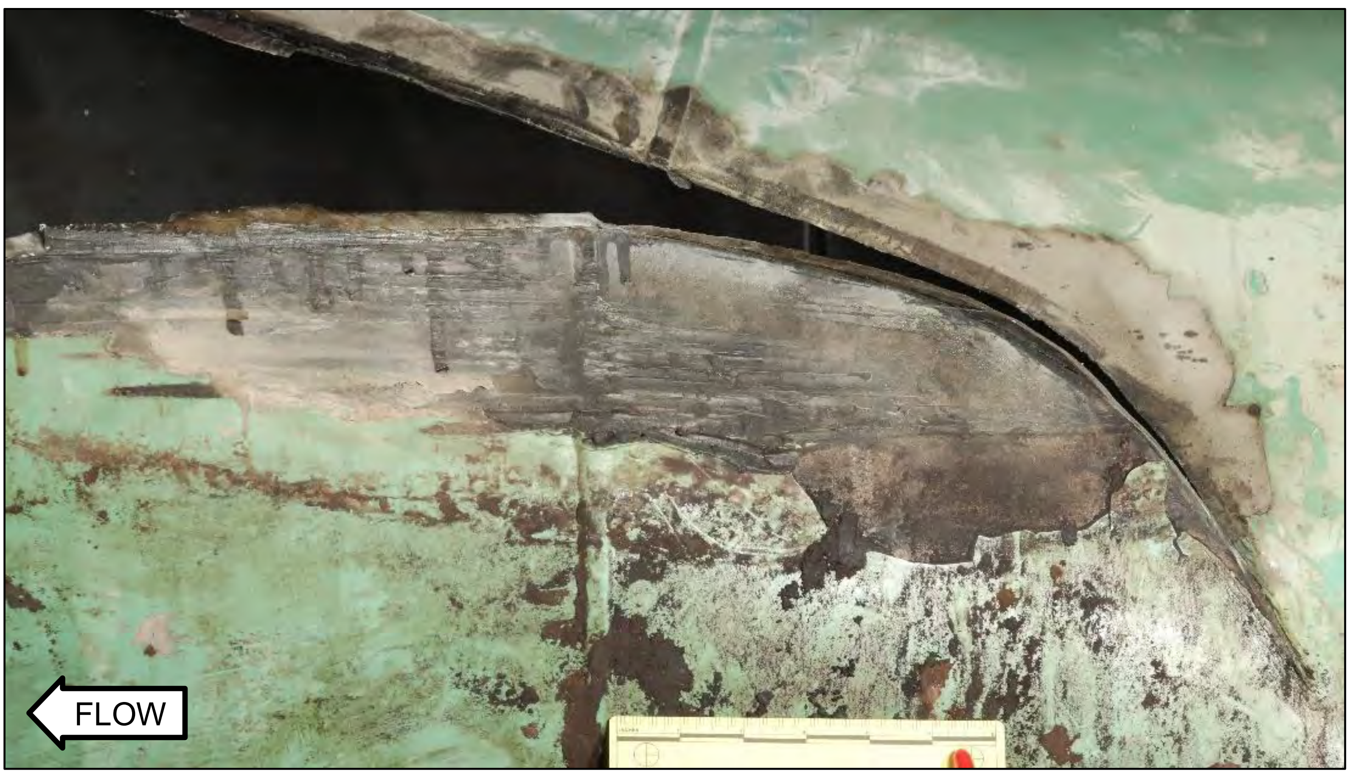

Figure 5. Sliding contact marks and missing coating on the surface adjacent to the left side of the fracture viewed as-received before cleaning.

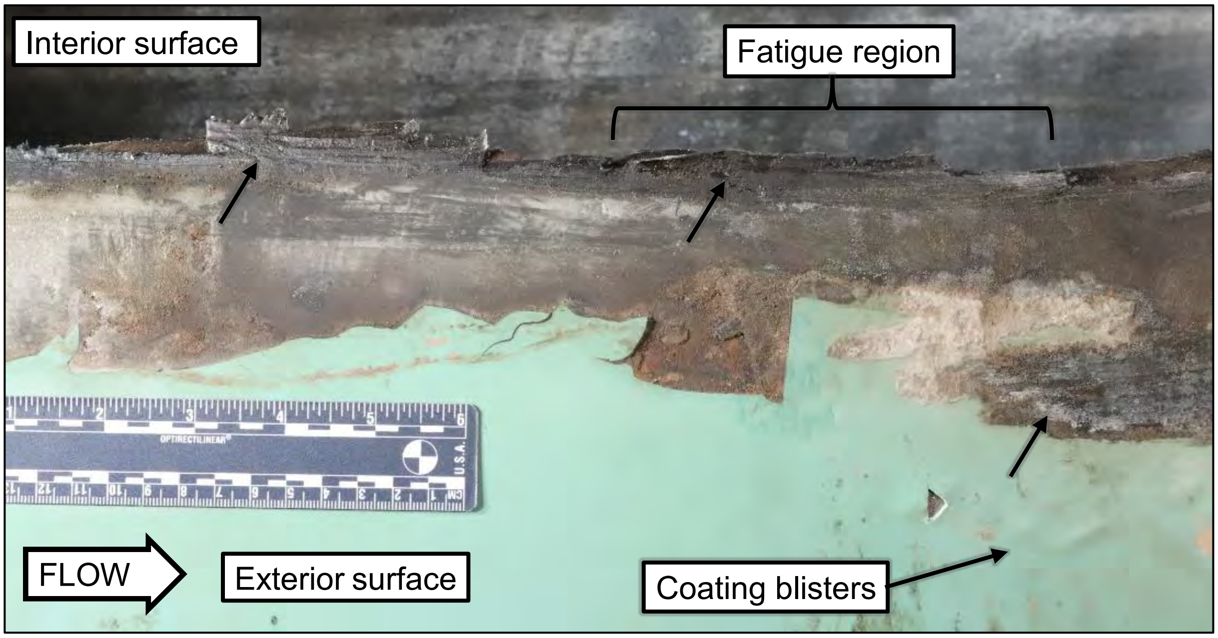

Figure 6. Pipe surface adjacent to the right side of the fracture. Unlabeled arrows indicate sliding contact marks on the surface.

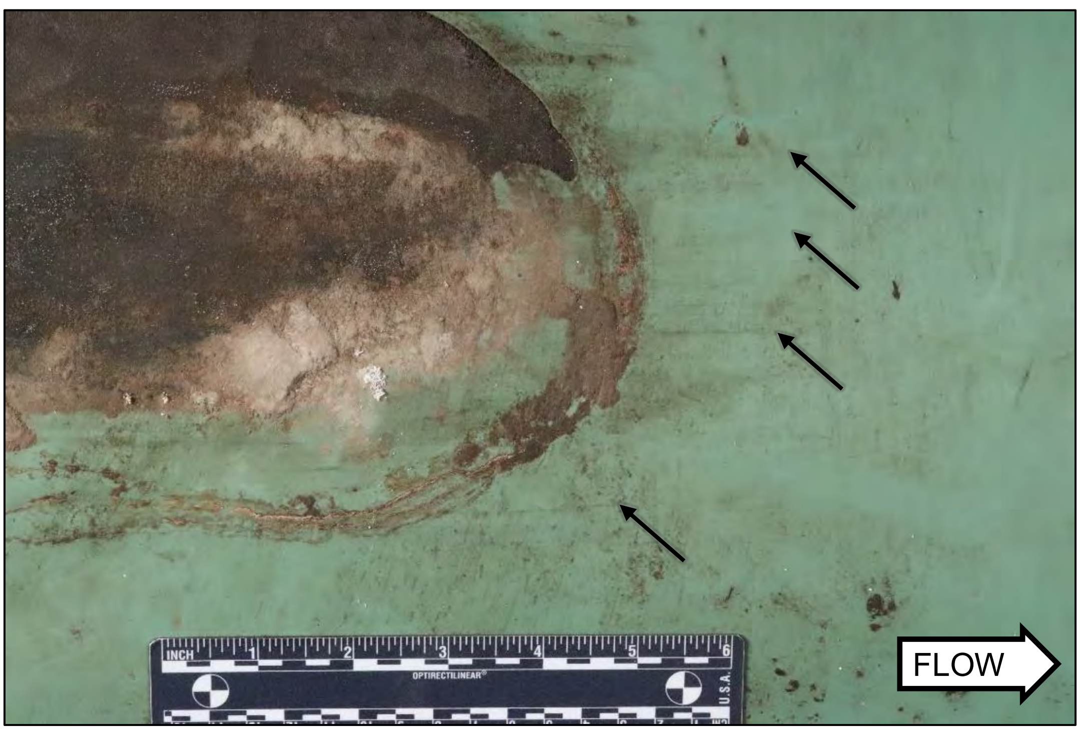

Figure 7. Downstream end of the sliding contact marks located at the top of the pipe. Unlabeled arrows indicate sliding contact marks on the exterior surface of the intact coating.

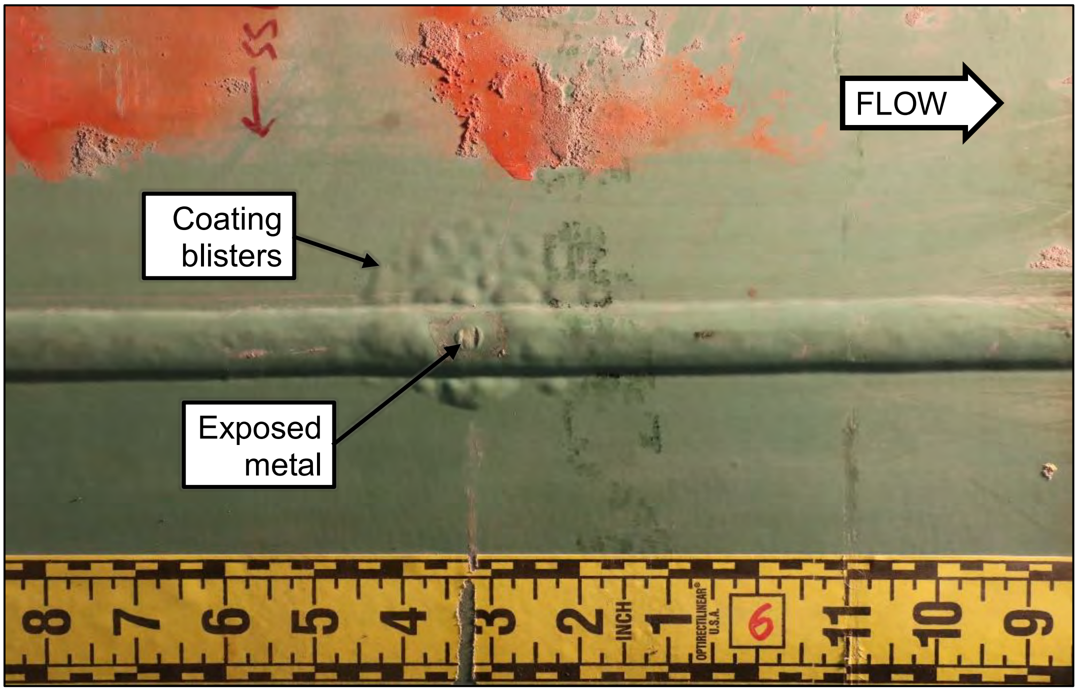

Figure 8. Isolated area of coating damage on the longitudinal seam approximately 69 inches downstream from the girth weld.

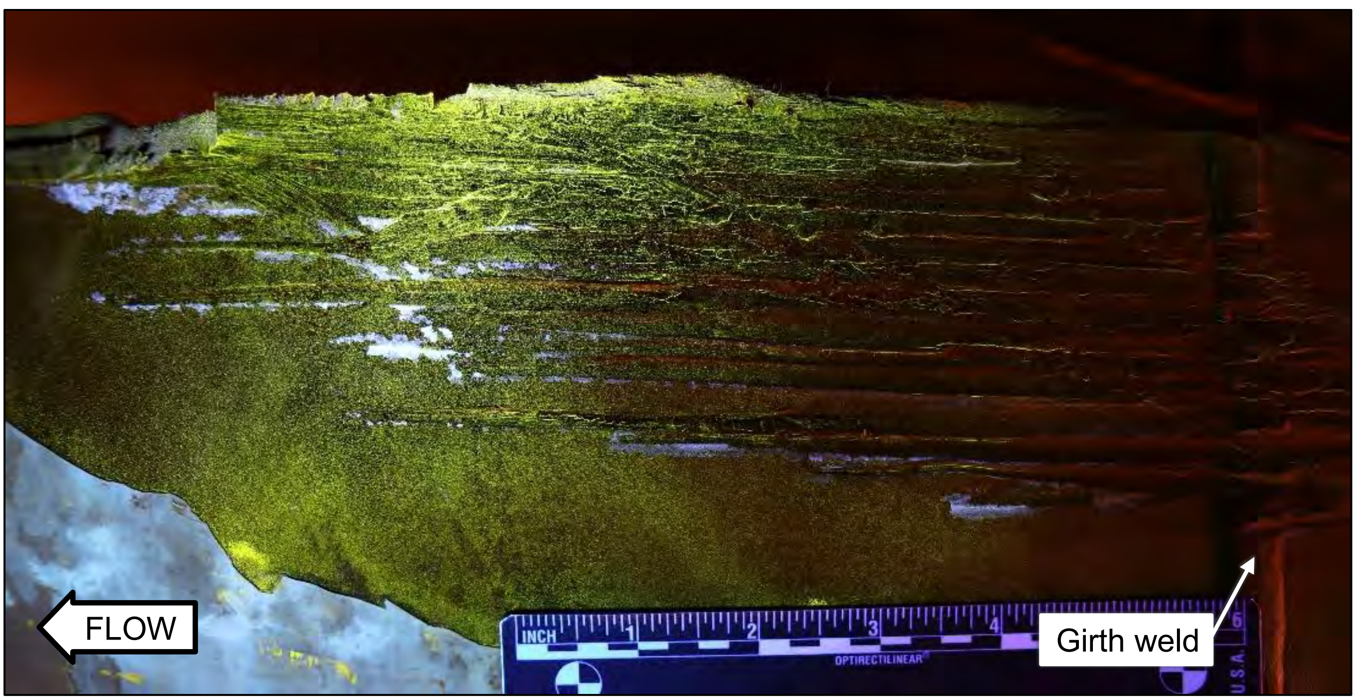

Figure 9. View of crack indications detected using fluorescent MPI in the area of sliding contact damage adjacent to the left side of the fracture.

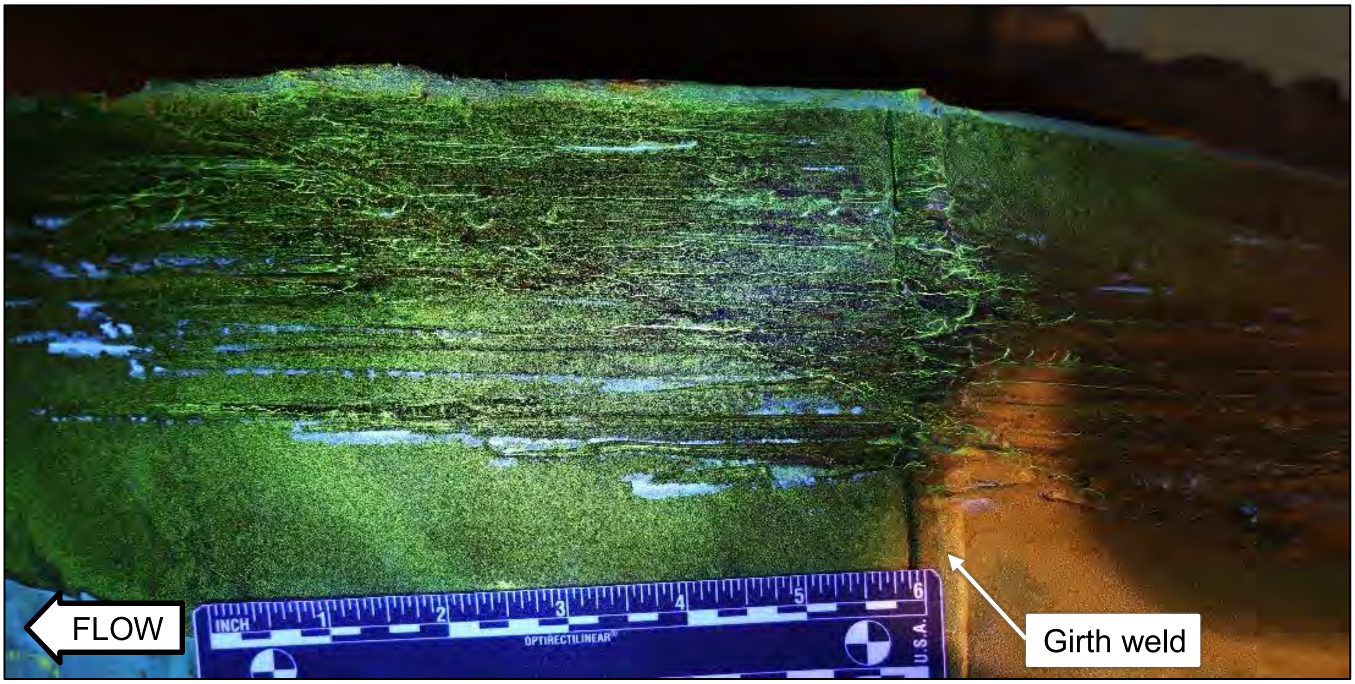

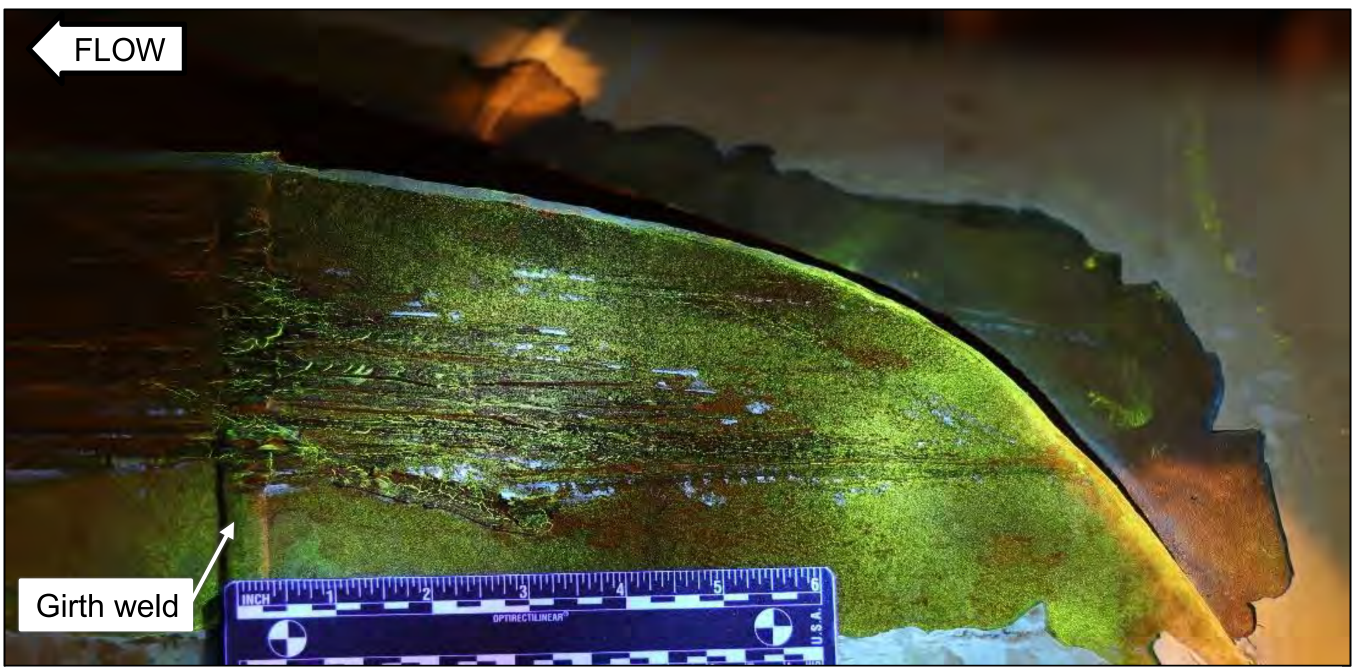

Figure 10. Views of crack indications detected using fluorescent MPI in the area of sliding contact damage adjacent to the left side of the fracture.

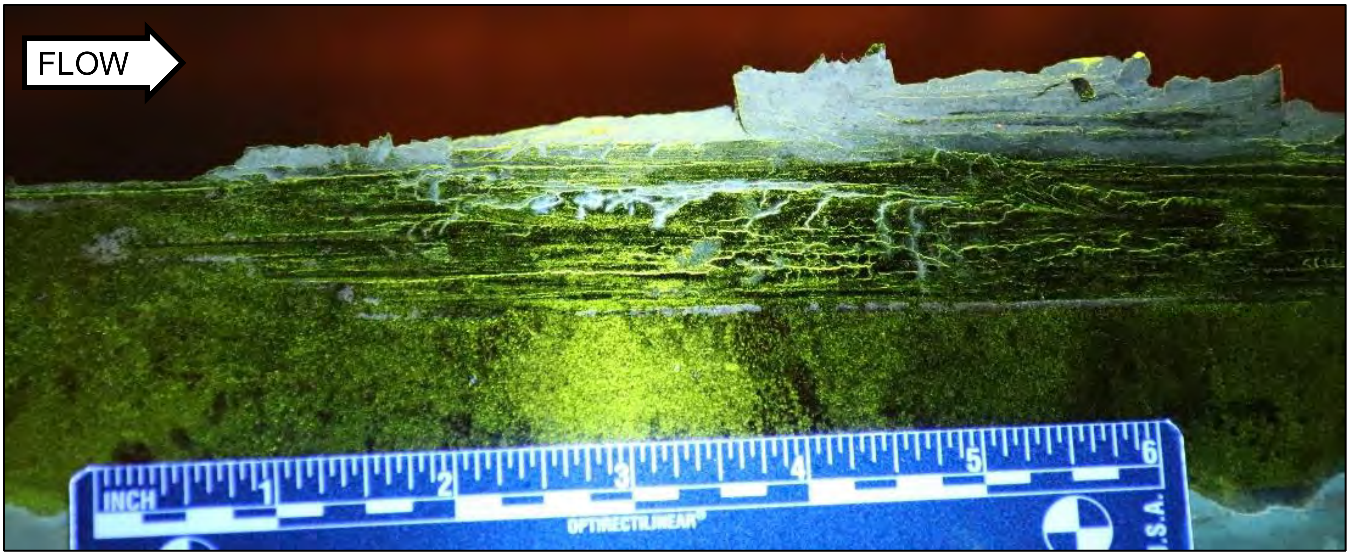

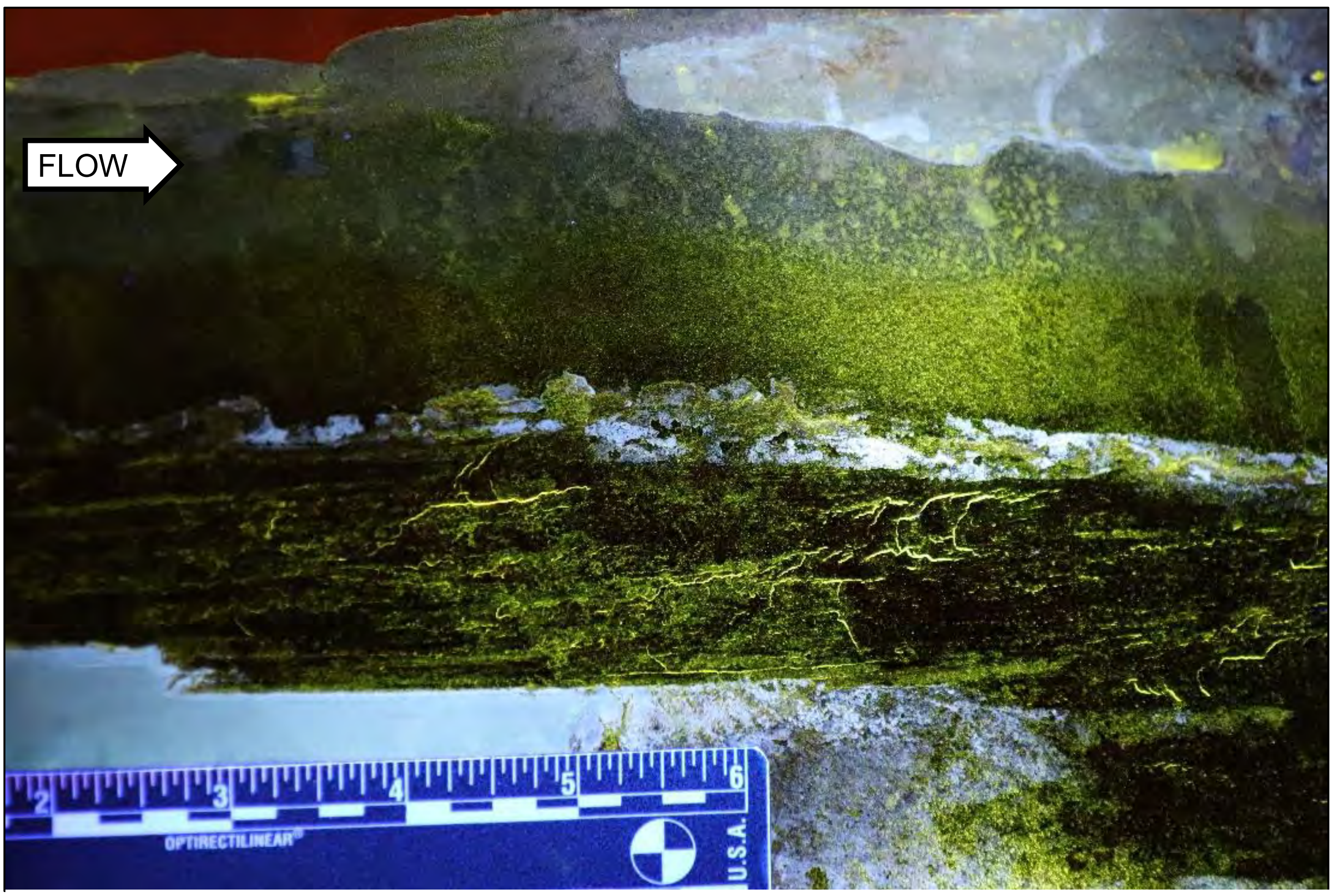

Figure 11. Views of crack indications detected using fluorescent MPI in the area of sliding contact damage adjacent to the right of the fracture approximately 10 inches downstream of the girth weld (upper image) and at the top of the pipe approximately 20 inches downstream of the girth weld (lower image).

Figure 12. View of the left side of the pipe after cleaning and before sectioning.

Figure 13. Overall view of the exterior surface after sectioning with the two sides of the fracture placed in close proximity. Dashed lines indicate the 12 o'clock position, and unlabeled brackets indicate the fatigue crack region.

Figure 14. Closer views of sliding contact marks on the pipe surface with the two sides of the fracture placed in close proximity. Brackets in the upper image indicate the fatigue region.

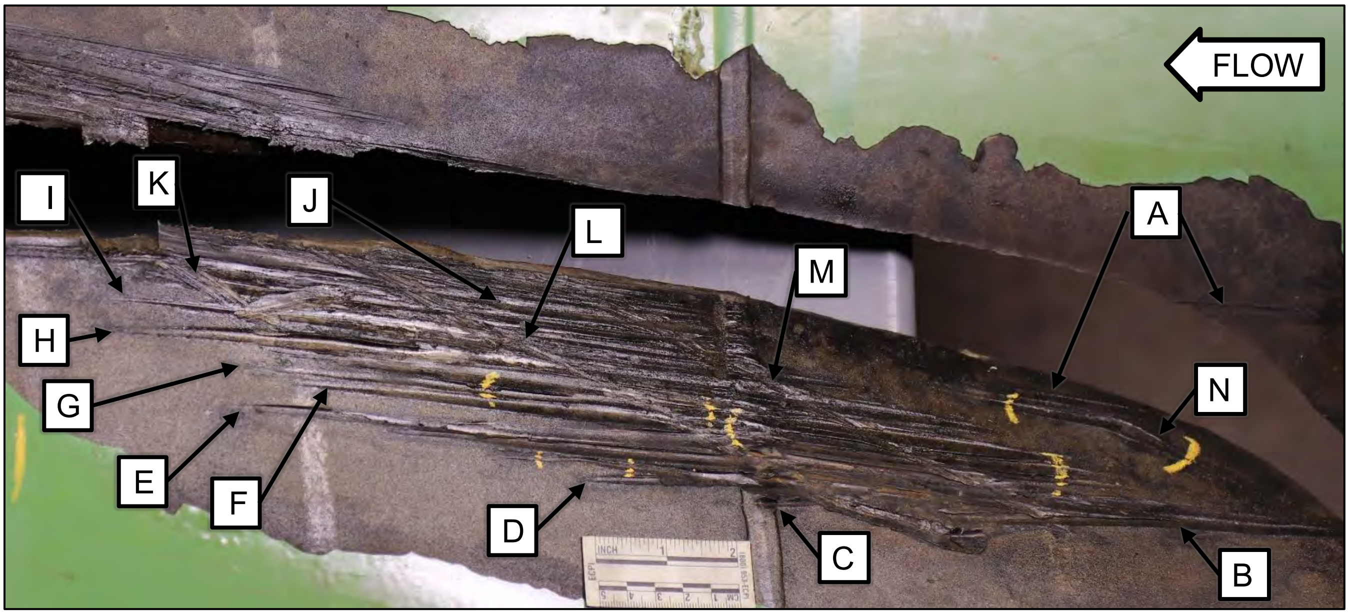

Figure 15. Sliding contact marks labeled for reference in the text.

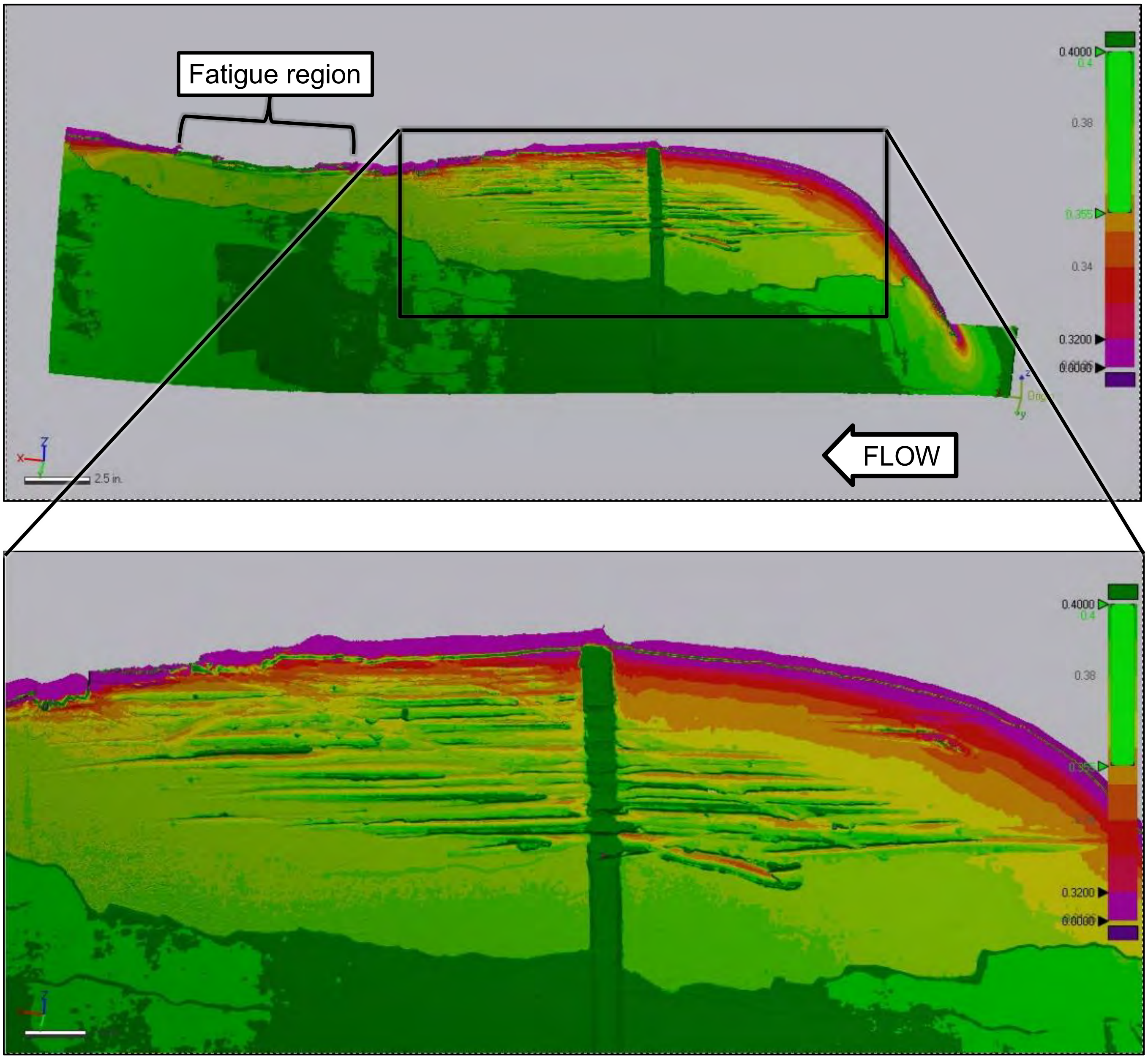

Figure 16. Thickness contour maps generated from a 3-dimensional laser scan of the pipe piece with the left side of the fracture.

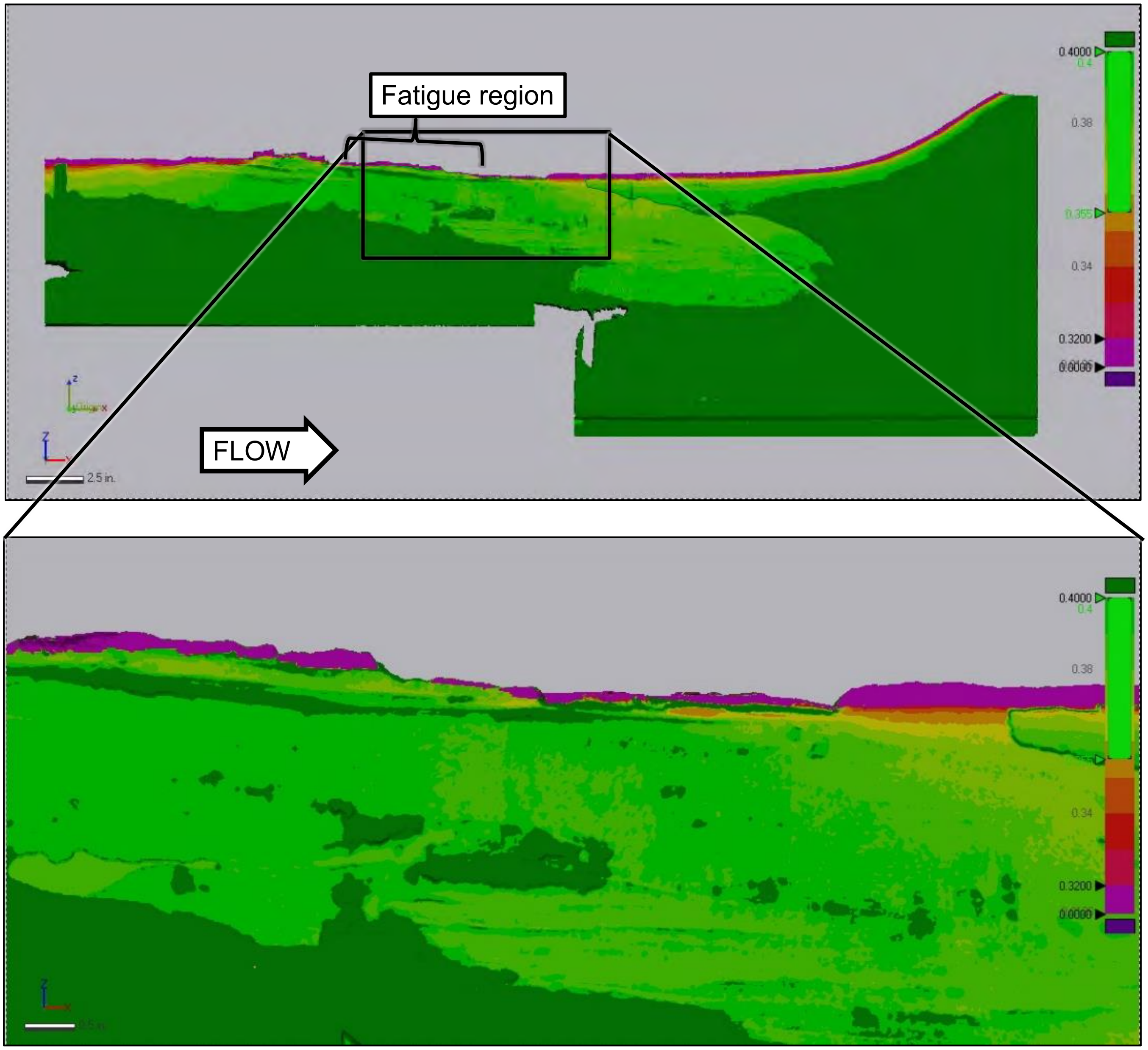

Figure 17. Thickness contour maps generated from a 3-dimensional laser scan of the pipe piece with the right side of the fracture.

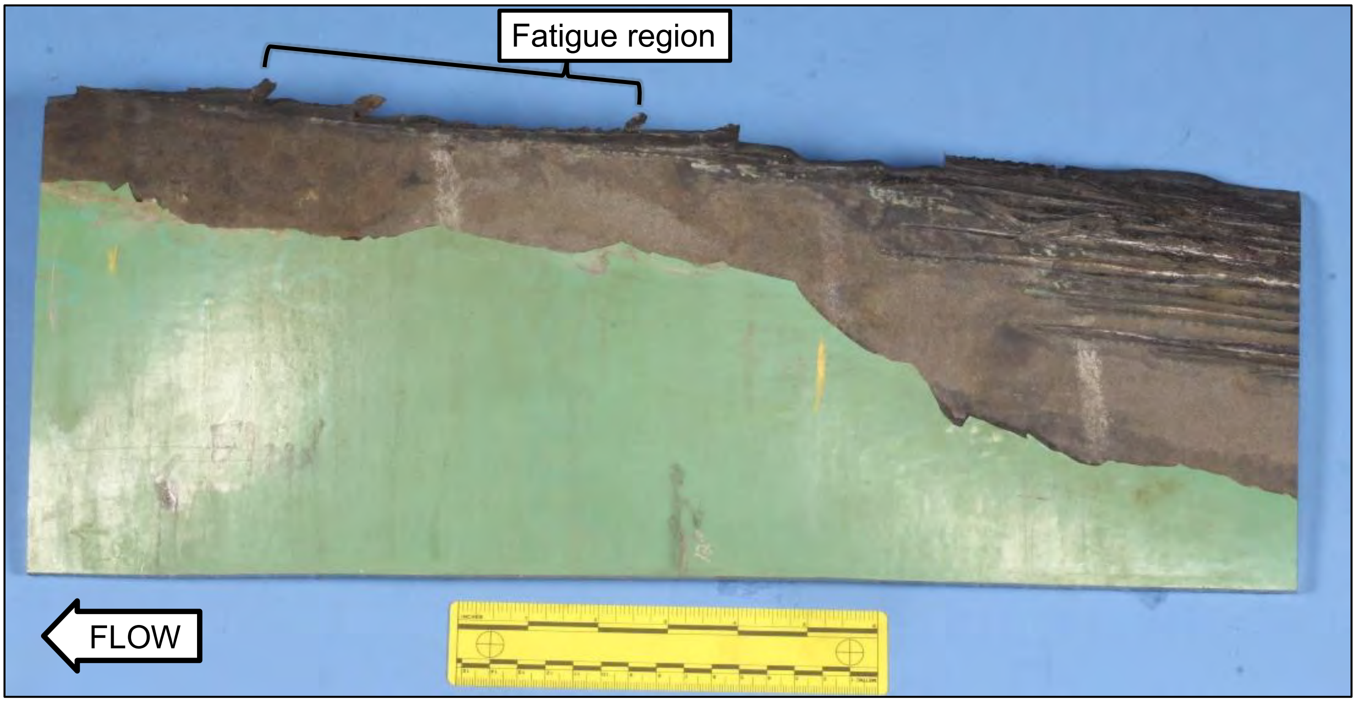

Figure 18. Piece with a portion of the left side of the fracture including the fatigue region and a portion of the sliding contact marks. The piece was cleaned using a soft-bristle brush and a solution of Alconox and water followed by an ethanol rinse.

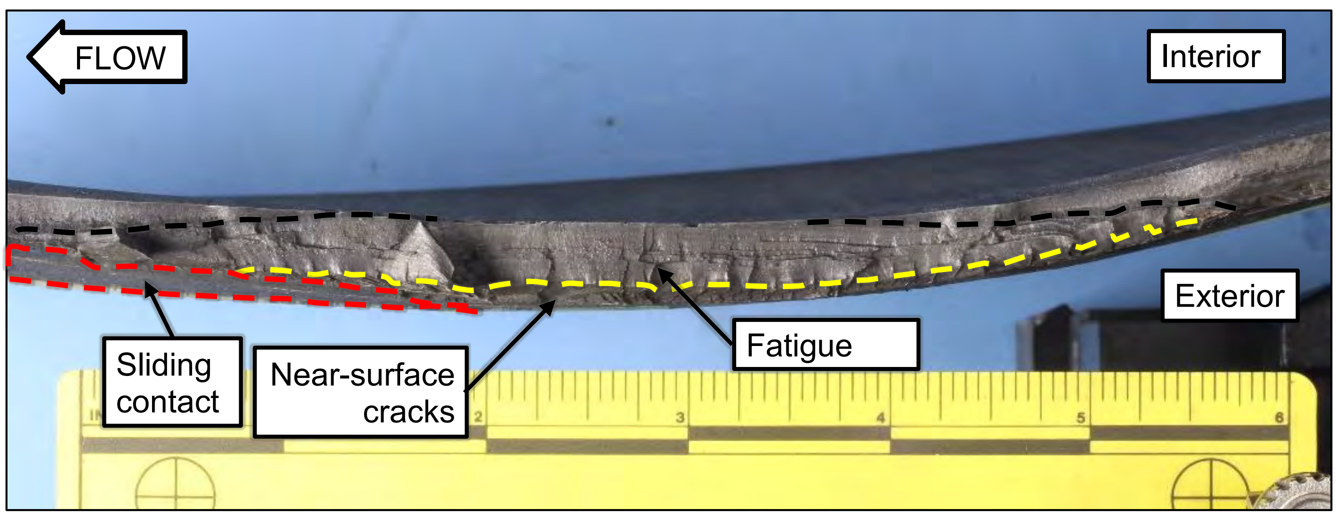

Figure 19. Close view of the fatigue region on the left side of the fracture after cleaning. Fatigue features emanated from near-surface cracks and extended to the boundary indicated with a black dashed line. The boundary of the near-surface cracks is indicated with a yellow dashed line. A portion of the area of the sliding contact damage on the exterior surface is also visible in this view, and the visible area is bounded by a red dashed line.

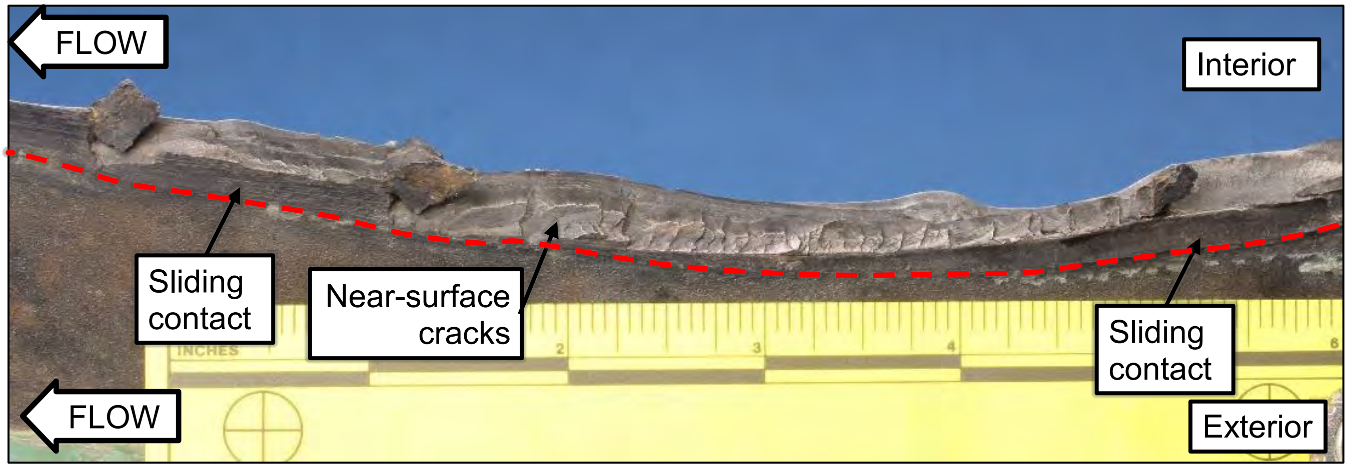

Figure 20. Oblique view of the fatigue region shown in the previous figure. A dashed line indicates the boundary of sliding contact damage observed on the exterior surface adjacent to the fracture.

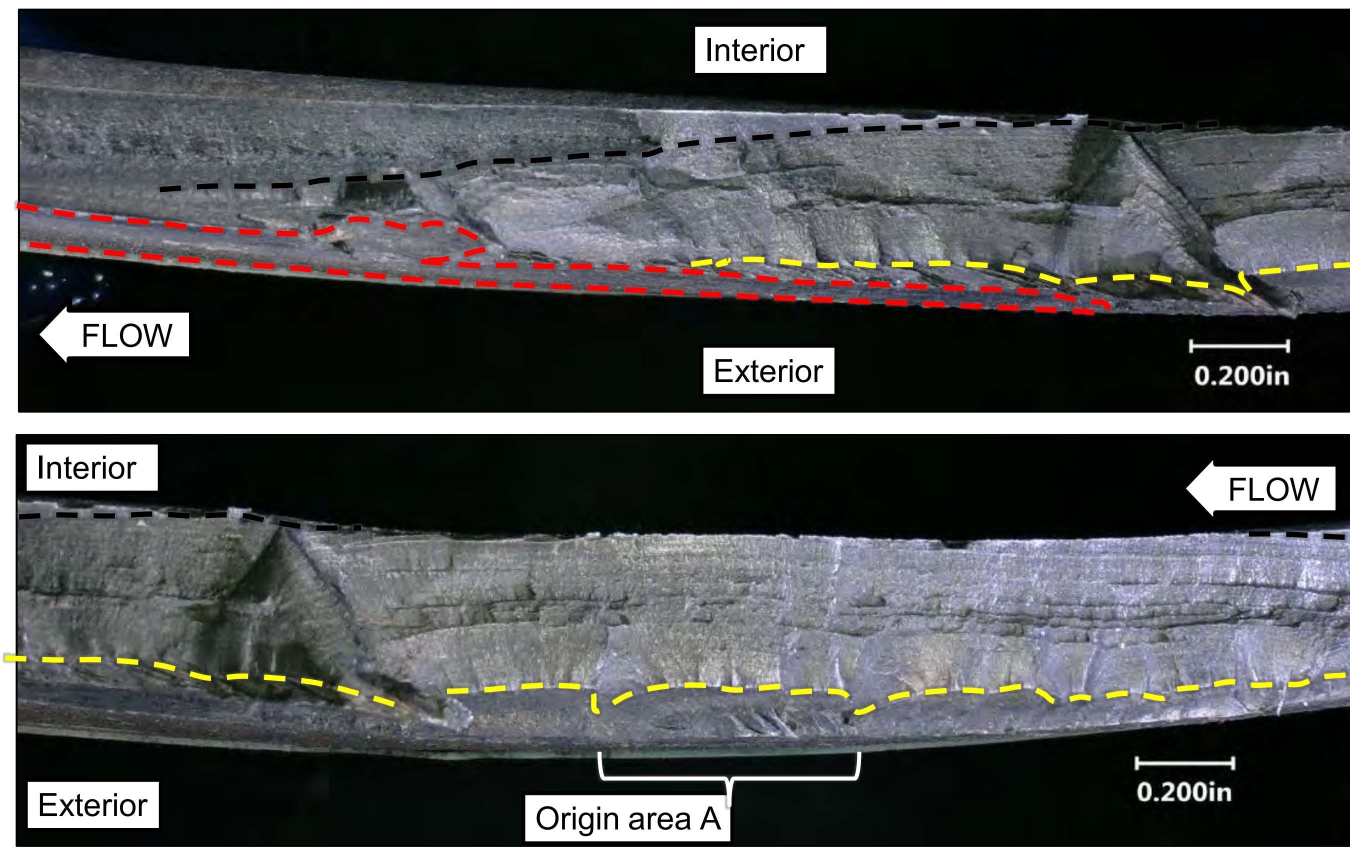

Figure 21. Optical images at higher magnification showing the downstream end (upper image) and middle portion (lower image) of the fatigue region (bounded by the black dashed lines), near-surface cracks (bounded by the yellow dashed lines), and visible portion of the sliding contact damage on the exterior surface (bounded by the red dashed line).

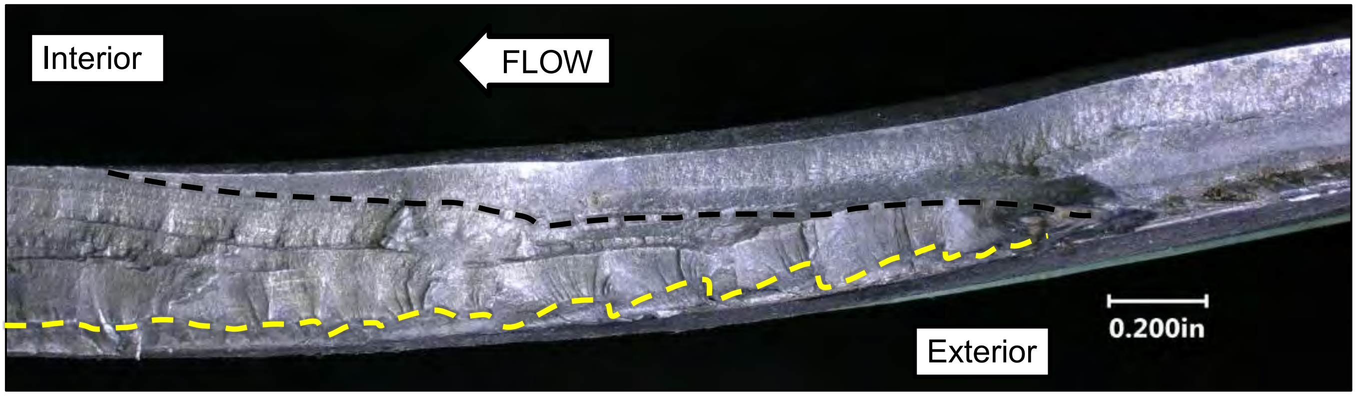

Figure 22. Optical image at higher magnification showing the upstream end of the fatigue region (bounded by the black dashed line) and the near-surface cracks (bounded by the yellow dashed line).

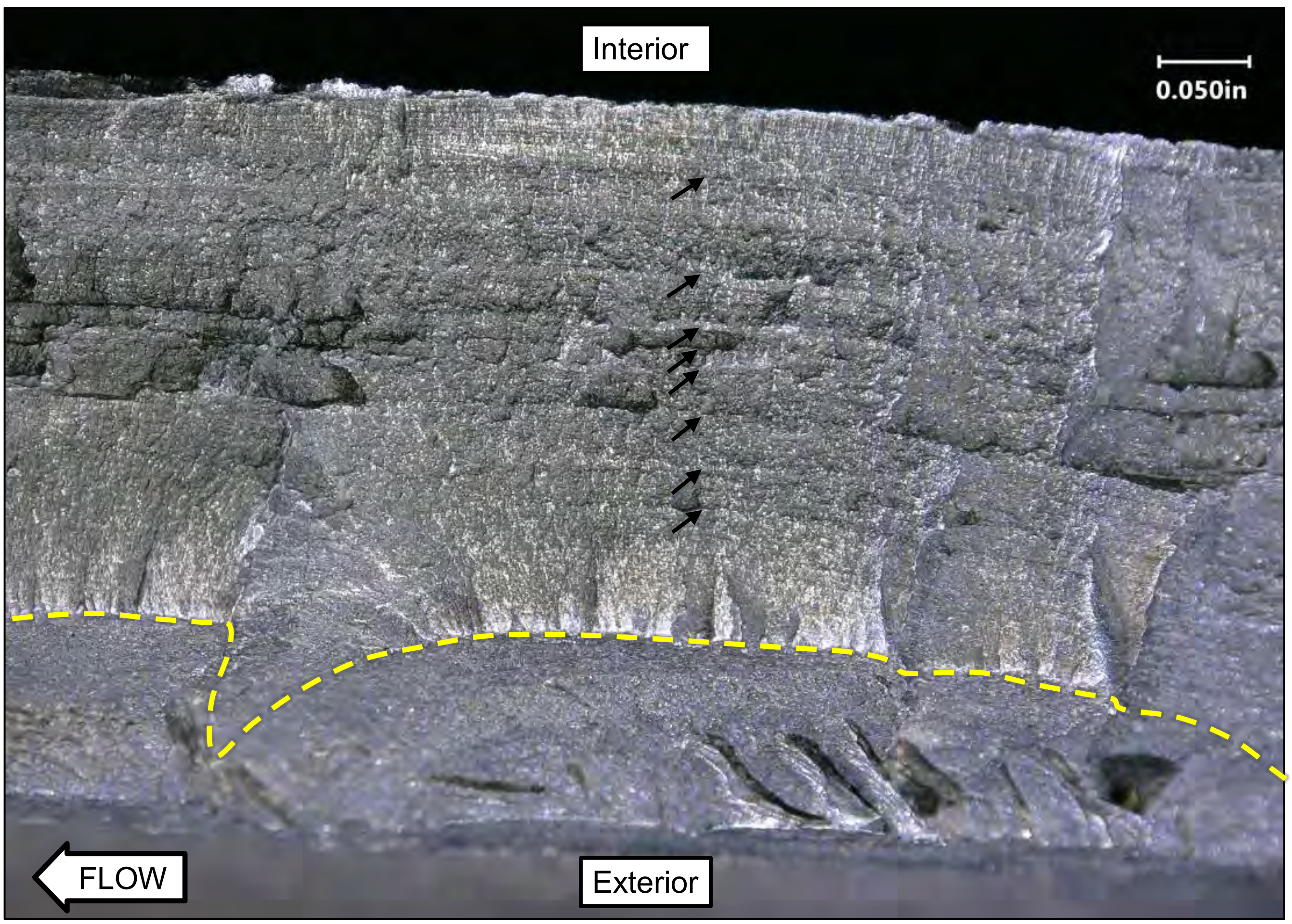

Figure 23. Optical image of the fatigue region at origin area A (see figure 21). Fatigue features emanated from near-surface cracks shown bounded by a yellow dashed line. Unlabeled arrows indicate relatively prominent crack arrest lines where emerging radial marks consistent with crack reinitiation were associated with the arrest line.

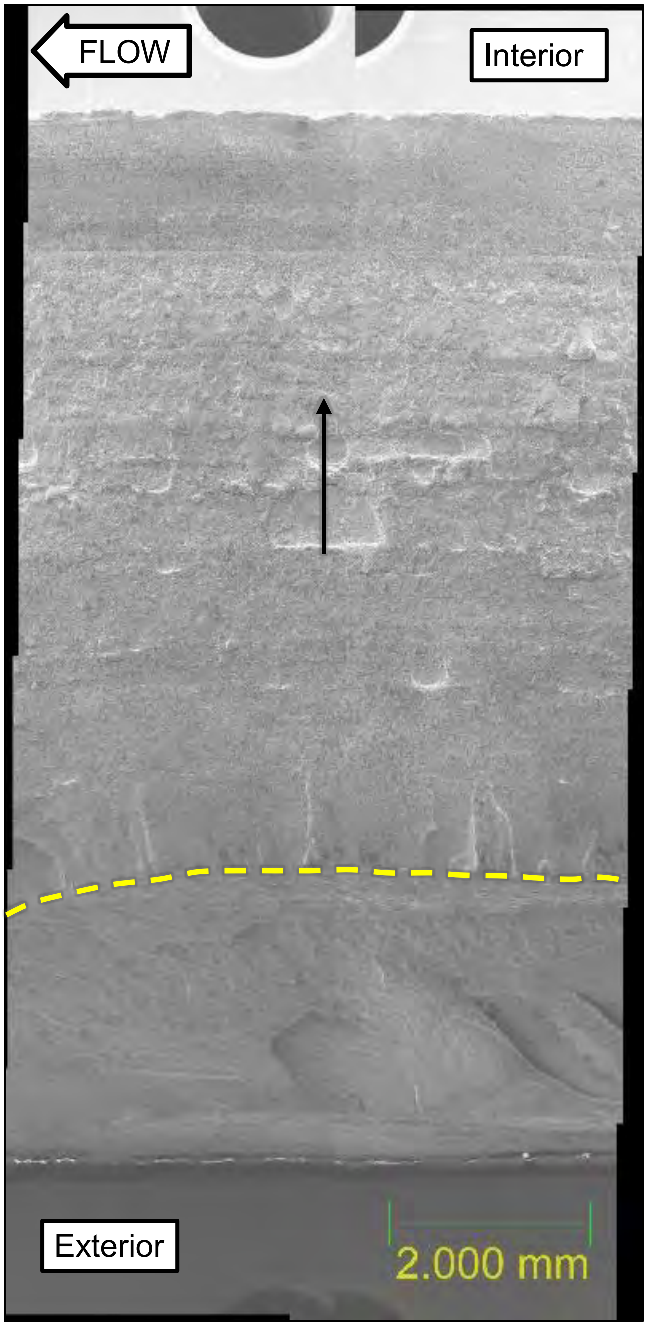

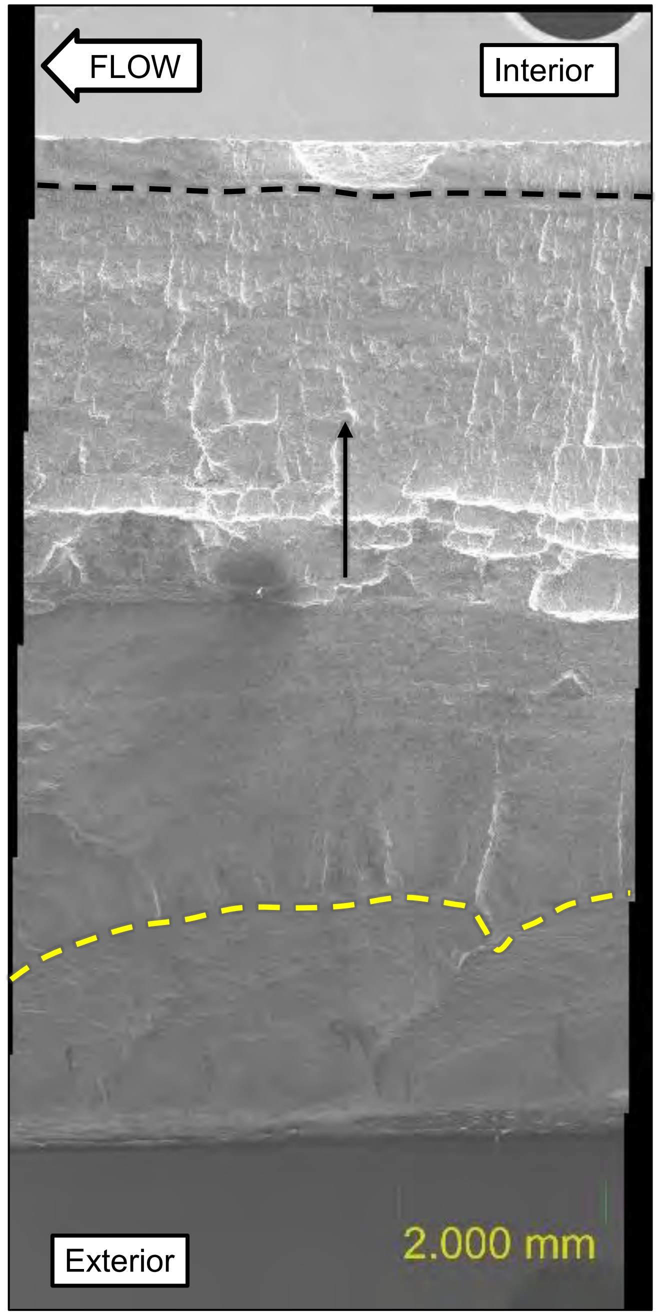

Figure 24. Series of SEM images of the fracture surface stitched together to form a montage image of fracture features at origin area A (left image) and at the adjacent origin area located upstream from origin area A (right image). Yellow dashed lines indicate the depth of the near-surface cracks, and a black dashed line in the right image indicates the extent of the fatigue region. In the left image, the fatigue region extends to the interior surface. Unlabeled arrows indicate the general direction of fatigue crack propagation from the near-surface crack boundary toward the interior surface.

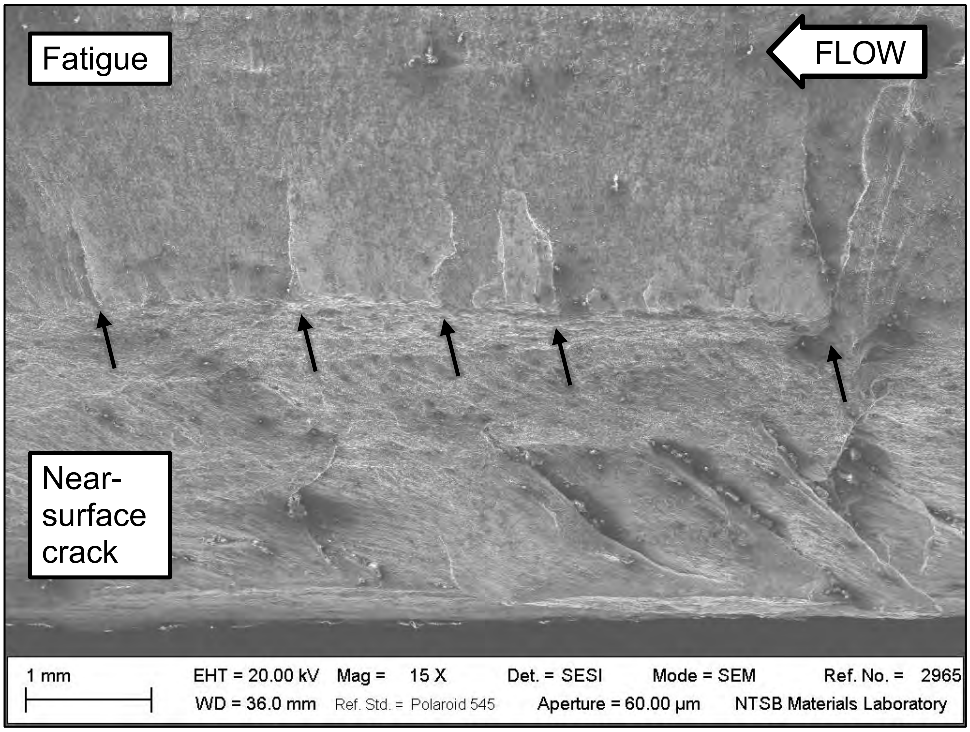

Figure 25. SEM image of the primary fatigue origin area emanating from a near-surface crack. Arrows point to ratchet marks located between origin areas.

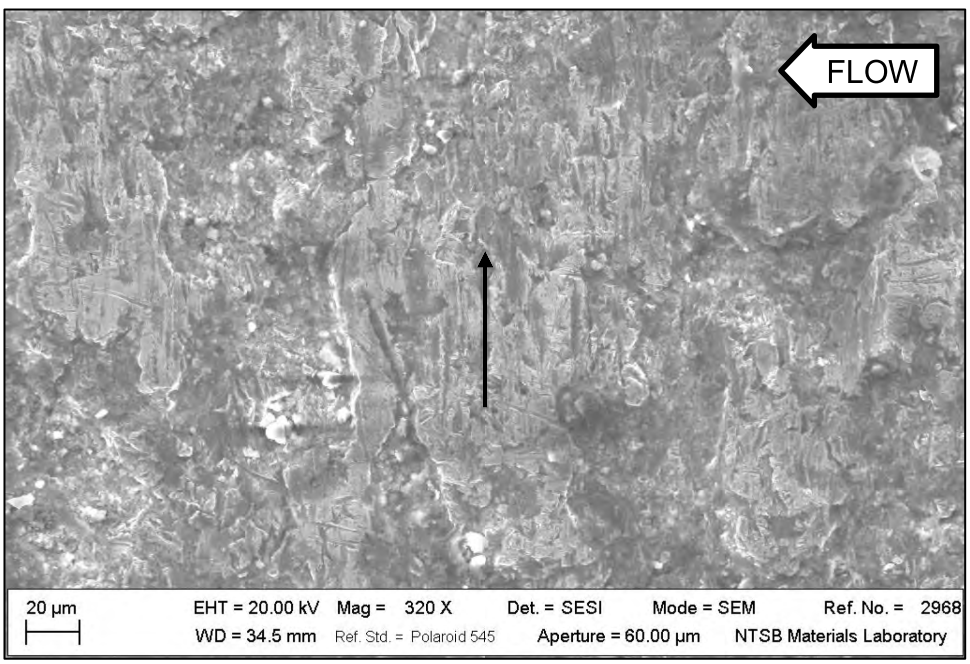

Figure 26. View of typical fracture features in the fatigue region. Fine fracture features were damaged by post-fracture abrasion. An unlabeled arrow indicates the direction of crack propagation.

Figure 27. Two SEM images stitched together to form a montage image of a near-surface crack at origin area A. The fracture surface was tilted so that the electron beam was approximately perpendicular to the near-surface crack fracture plane. A yellow dashed line indicates the extent of the near-surface crack. Sliding contact marks are also visible on the exterior surface as indicated. An unlabeled arrow indicates the direction of fatigue crack propagation emanating from the near-surface crack boundary.

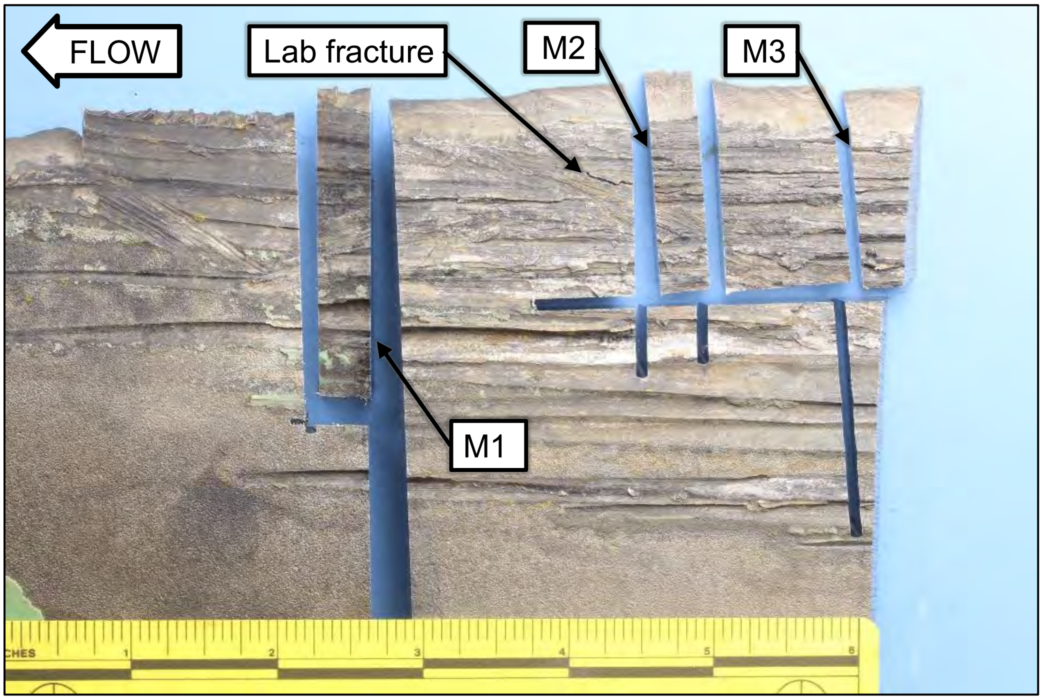

Figure 28. Area of sliding contact marks adjacent to the left fracture that was sectioned for metallographic examination of mounts M1, M2, and M3, for a lab fracture, and for SEM/EDS examination of the exterior surface.

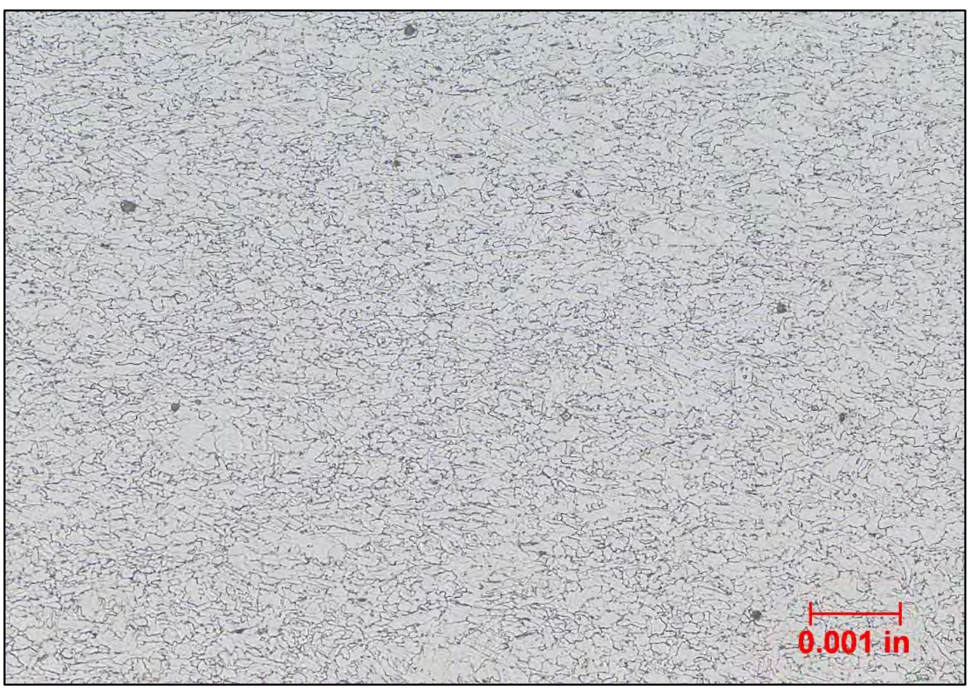

Figure 29. Typical microstructure of the pipe material (etched with 4% nital).

Figure 30. Micrograph of mount M2 at the exterior surface in an area of sliding contact. Some areas of the sliding contact had material at the surface that etched differently as indicated with an unlabeled bracket in this micrograph (etched with 4% nital).

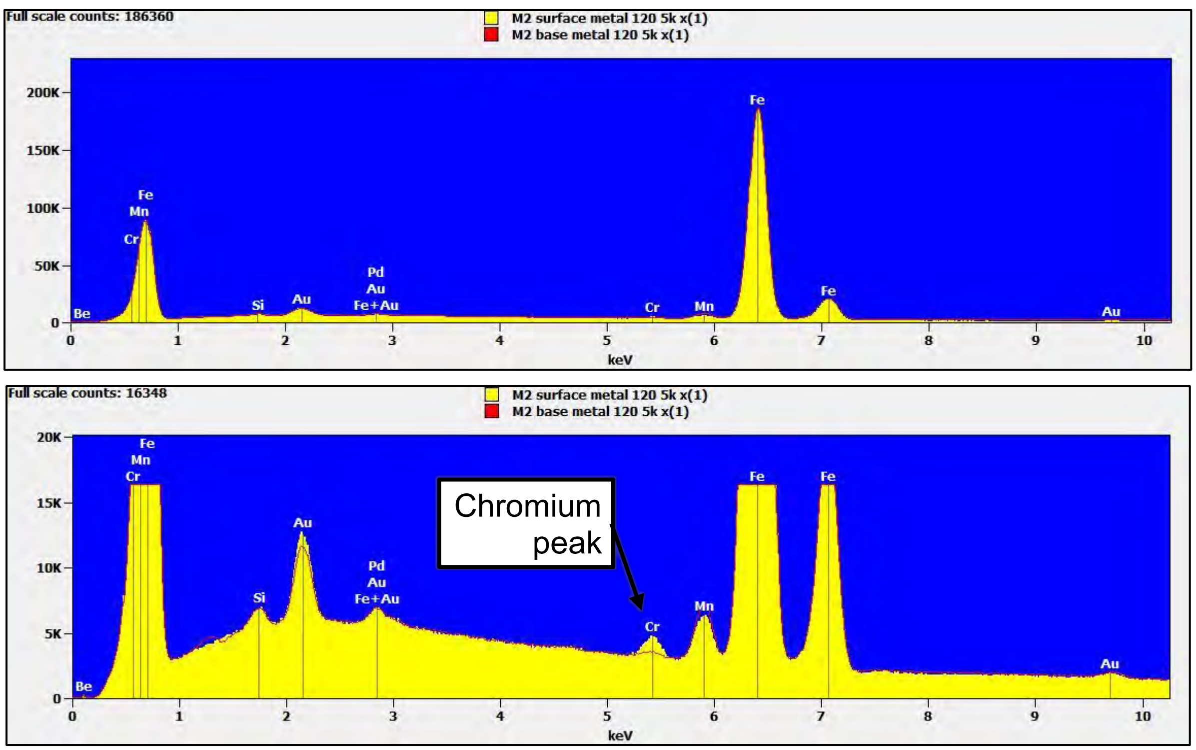

Figure 31. EDS spectrum of the surface material (yellow areas) compared to the spectrum for the underlying pipe material (red outline) in mount M2 after coating with a thin layer of gold/palladium. The upper image shows the spectrum at full scale, and the lower image shows the same data with the scale of the vertical axis reduced to highlight smaller peaks.

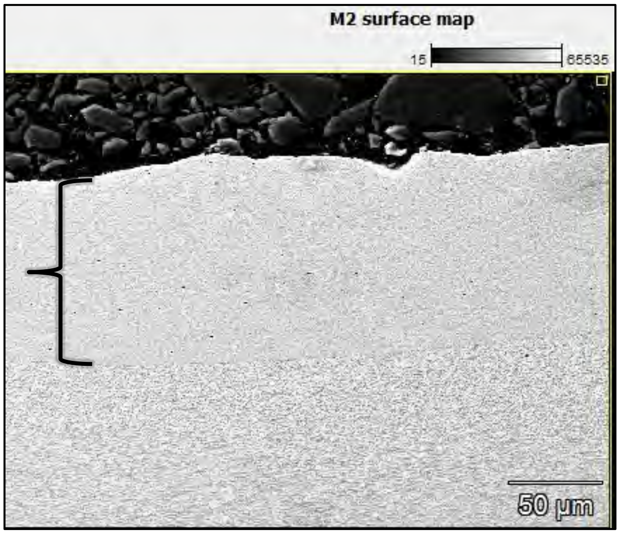

Figure 32. SEM image using the backscattered electron detector showing the area of mount M2 that was scanned using EDS mapping. An unlabeled bracket indicates the layer of deposited metal.

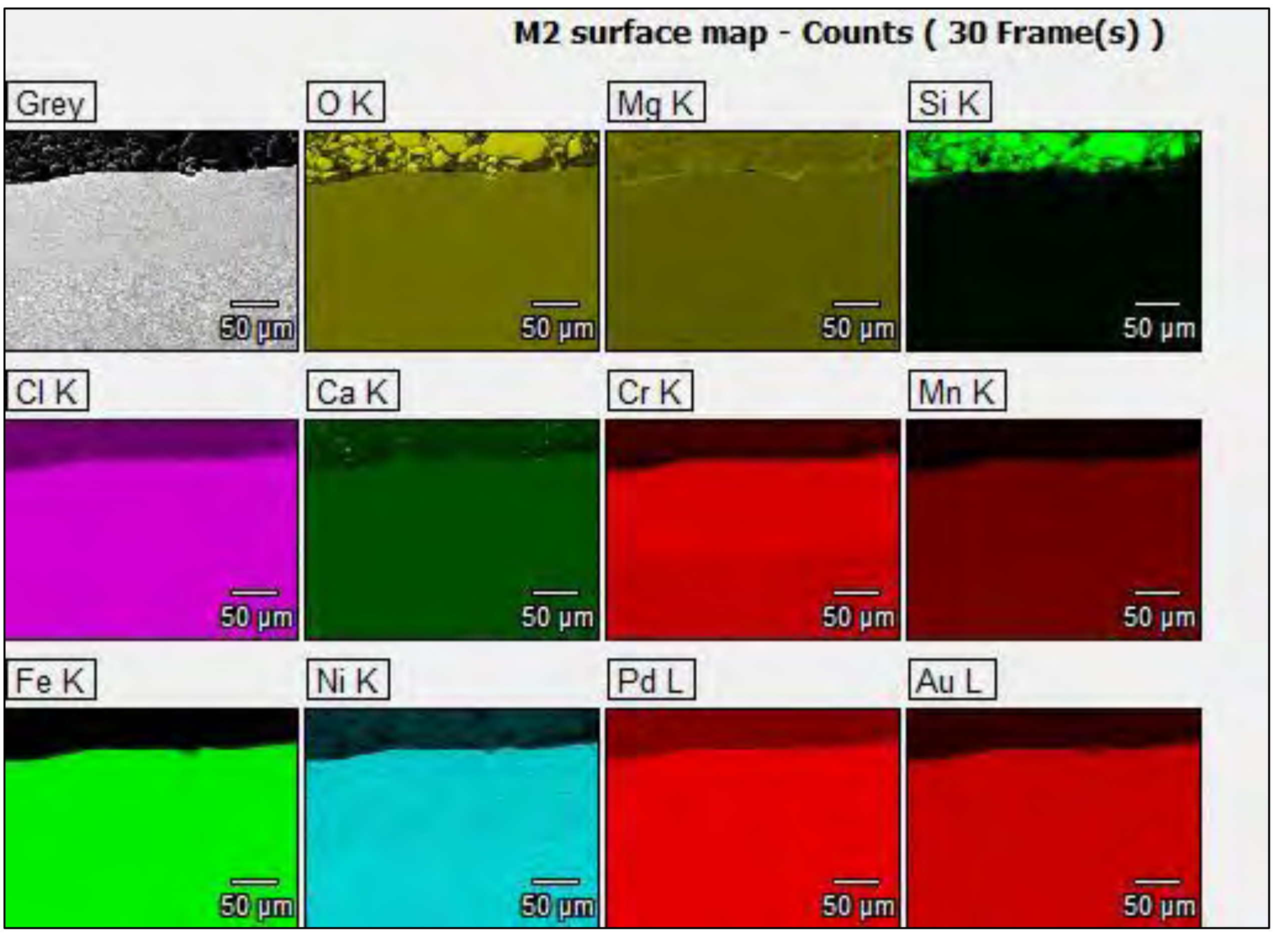

Figure 33. EDS maps of elements detected in the area shown in figure 32. See figure 34 for closer views of the maps for chromium and manganese. The specimen was coated with a thin layer of a gold/palladium alloy for SEM examination.

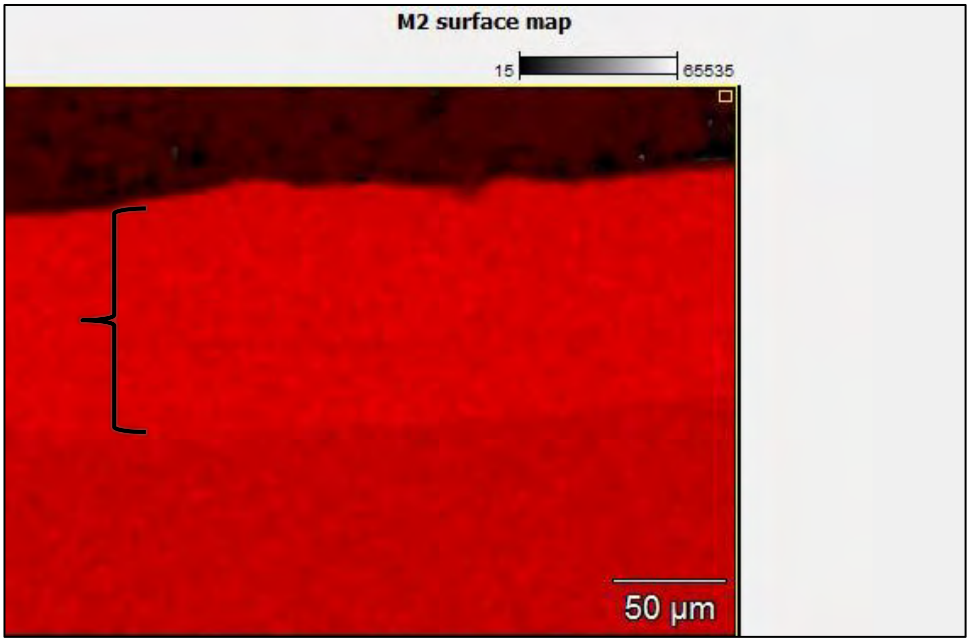

Figure 34. EDS map for chromium in the area shown in figure 32. An unlabeled bracket indicates the surface deposit where higher levels of chromium were detected as evident by higher brightness.

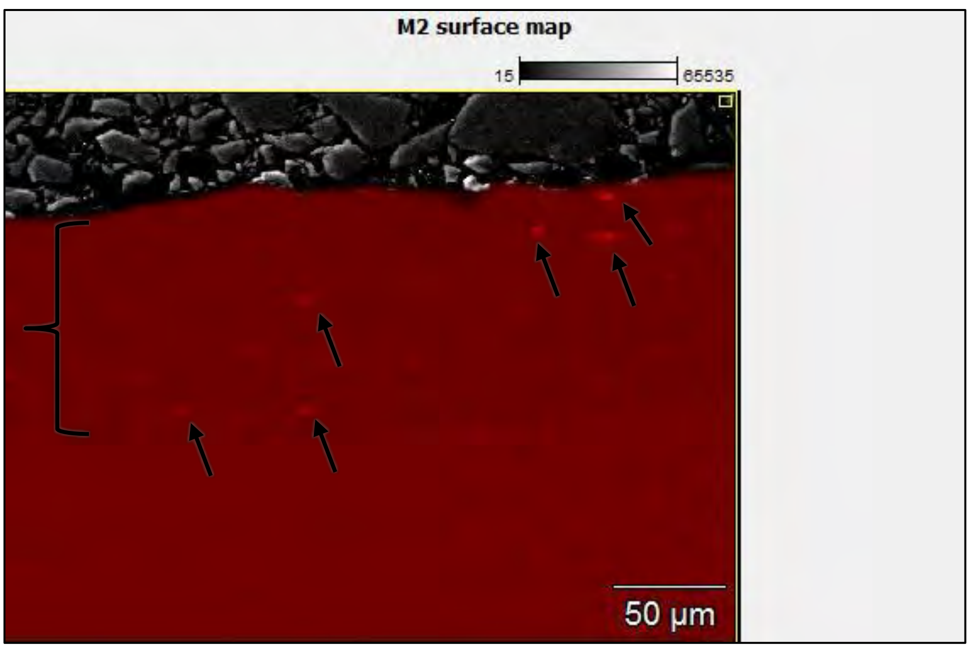

Figure 35. EDS map for manganese in the area shown in figure 32. An unlabeled bracket indicates the surface deposit which generally appeared slightly darker than the underlying pipe material. Bright spots (indicated with arrows) consistent with concentrations of manganese (likely manganese sulfide precipitates) were present in the surface deposit but not in the underlying pipe material.

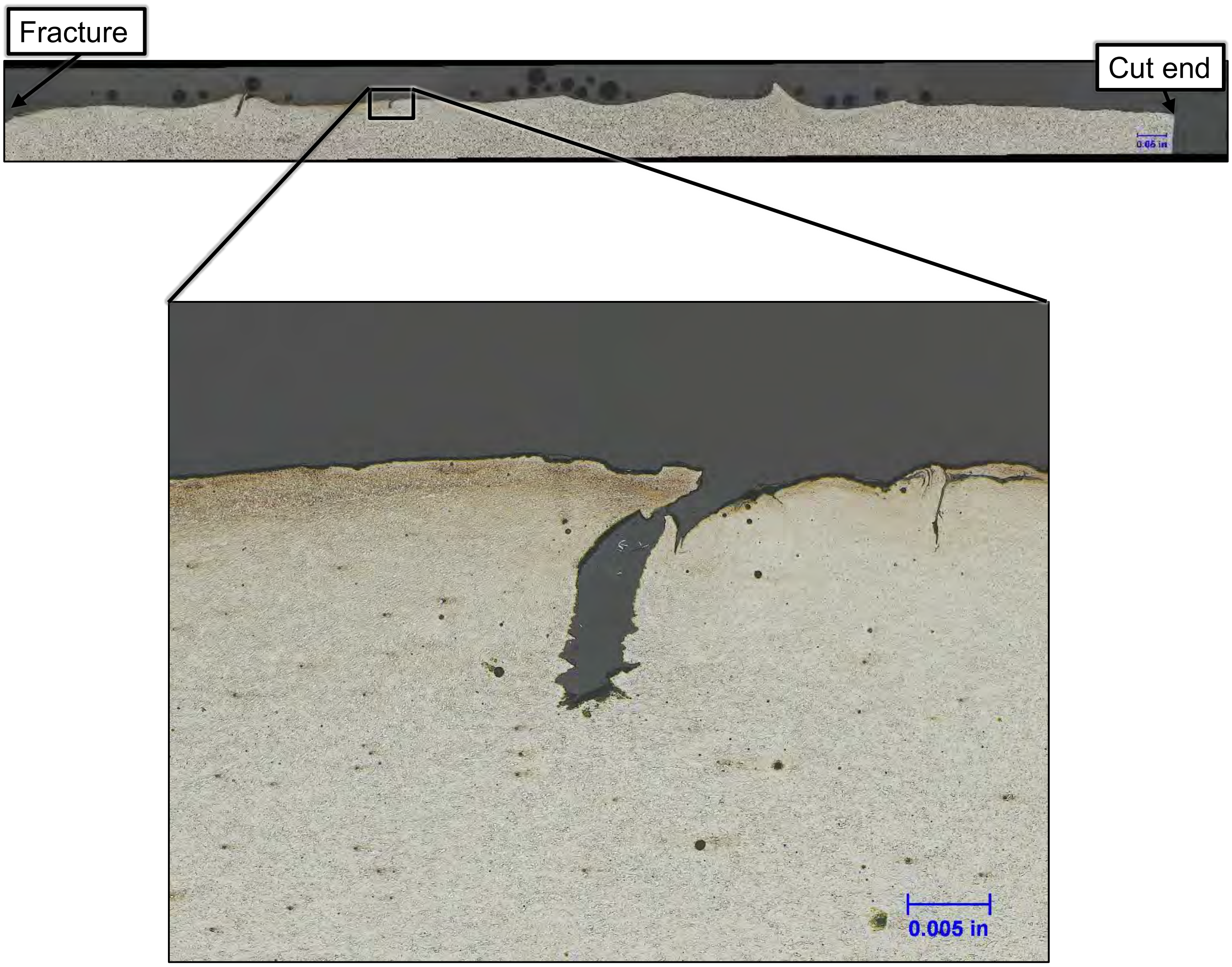

Figure 36. Stitched montage of micrographs of mount M1 showing the pipe exterior surface profile (upper image) with a detail image of one of the near-surface crack profiles (lower image).

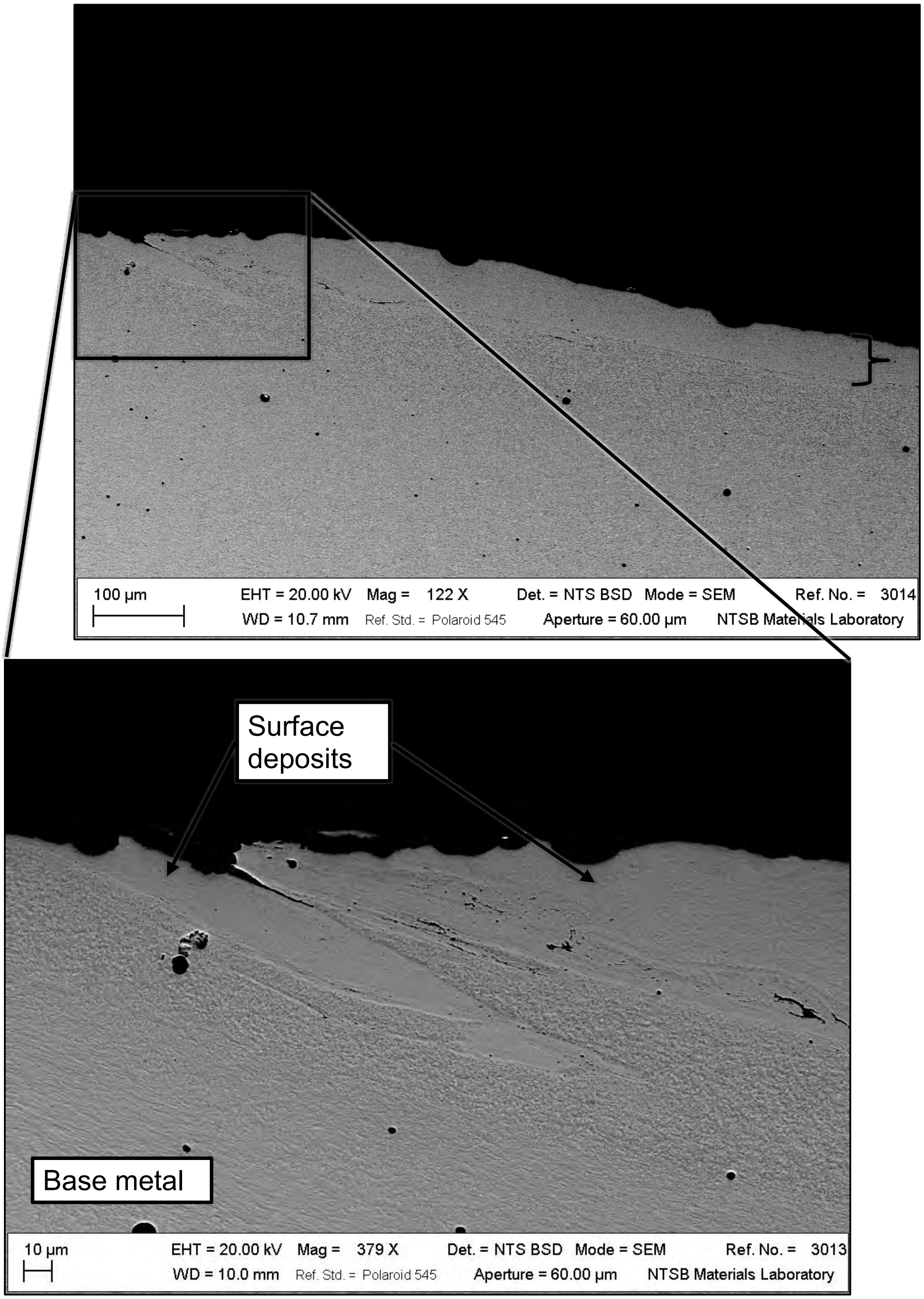

Figure 37. SEM image of mount M1 using the backscattered electron detector showing the microstructure near the surface in the sliding contact area. An unlabeled bracket in the upper image indicates a surface layer with higher chromium relative to the base metal and appearing smoother and slightly lighter gray. In some areas, overlapping layers of deposits were present such as in the location shown in the lower image. (Etched with 4% nital.)

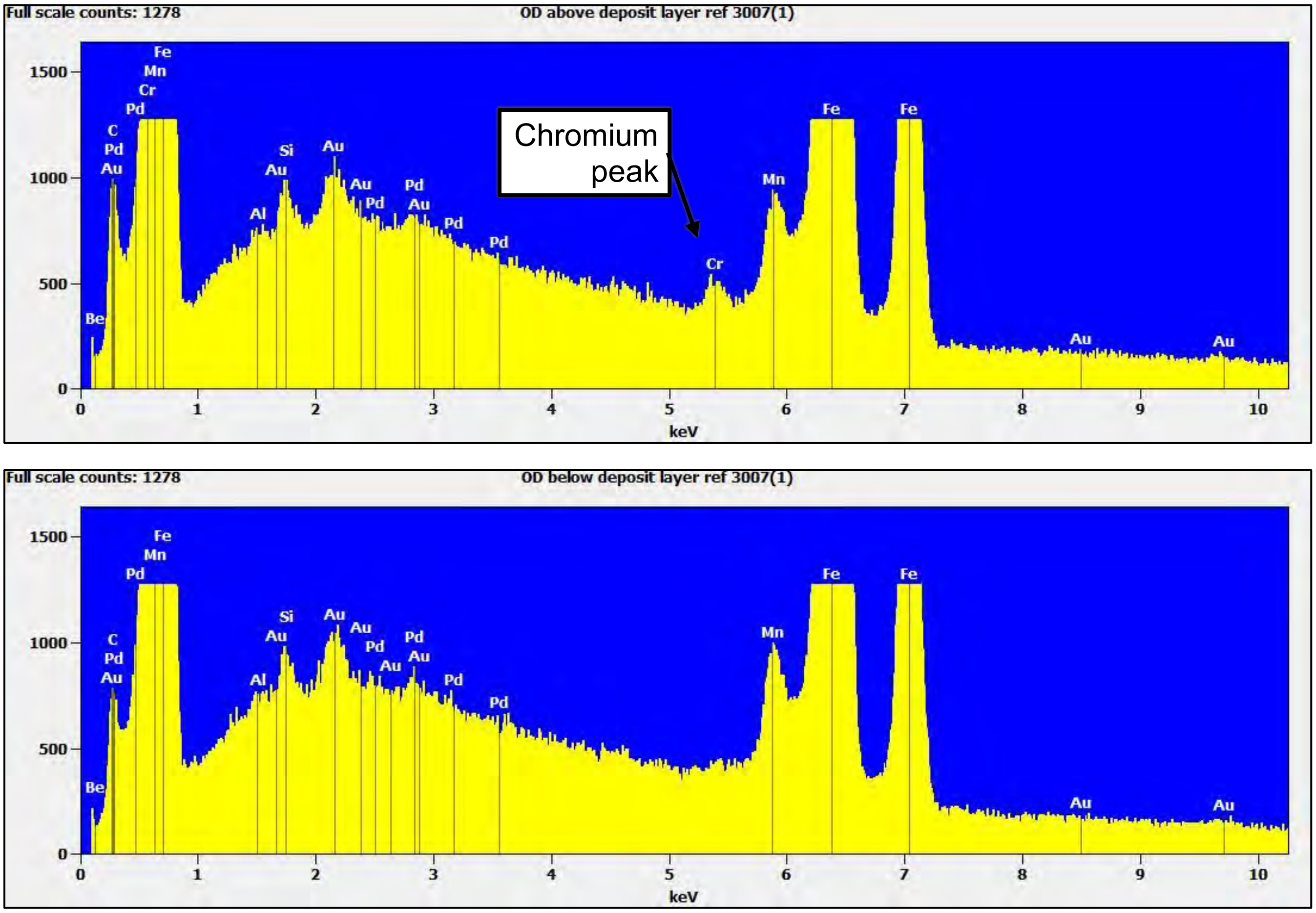

Figure 38. EDS results on sample M1 (coated with gold and palladium to avoid charging issues from the nonconductive mount) showing a distinct chromium (Cr) peak for the surface deposit (upper spectrum) versus the adjacent base material (lower spectrum).

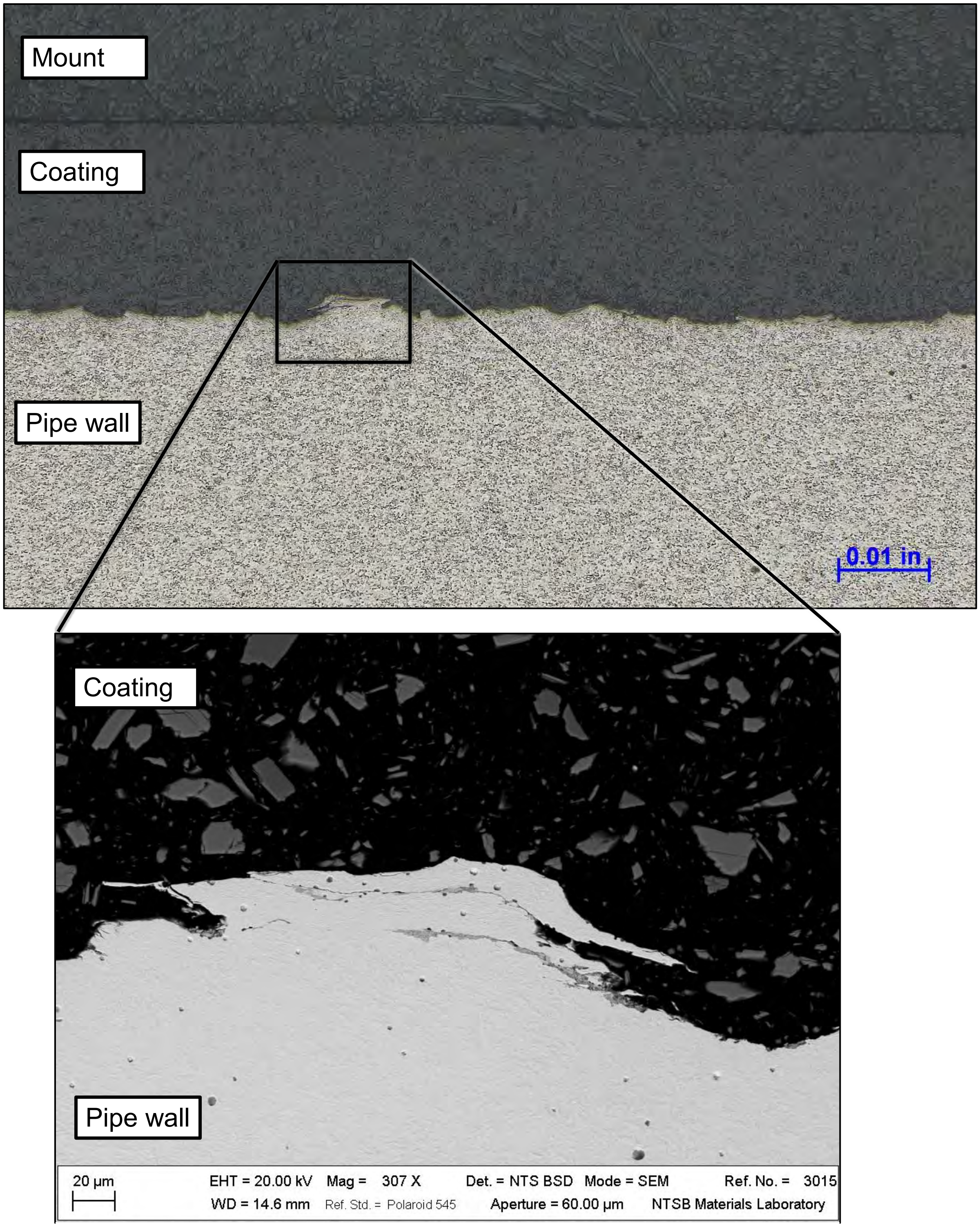

Figure 39. Metallographic cross-sections of a sample from an area where the coating was intact. The exterior surface of the pipe was imaged using the metallograph (upper image) and in the SEM using the backscattered electron detector (lower image). No layer of higher chromium was present. (Etched with 4% nital.)

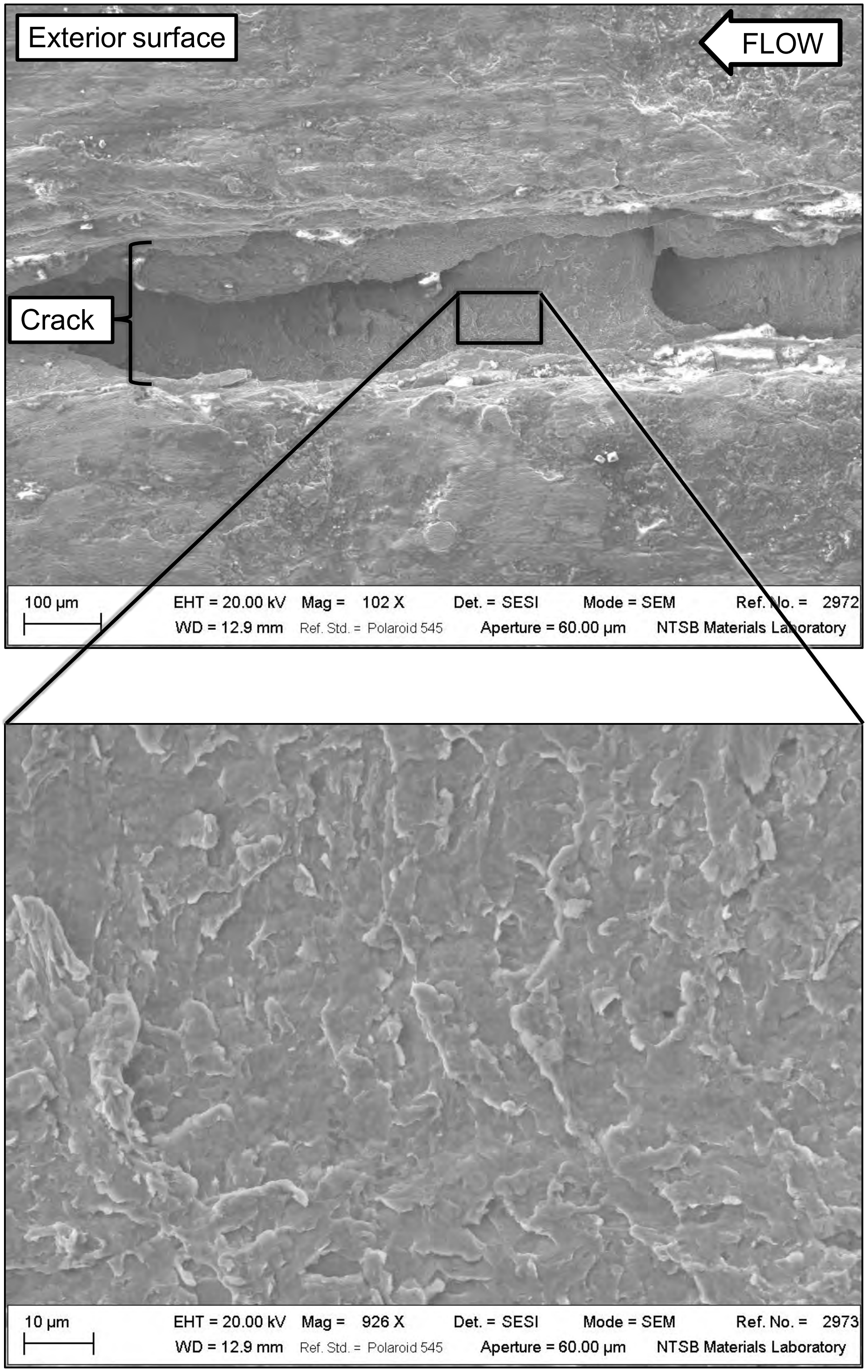

Figure 40. SEM image of a crack opening in an area of sliding contact on the exterior surface of the piece between mounts M2 and M3 (see figure 28). Fracture features had a transgranular appearance with tear-ridges consistent with quasi-cleavage fracture.

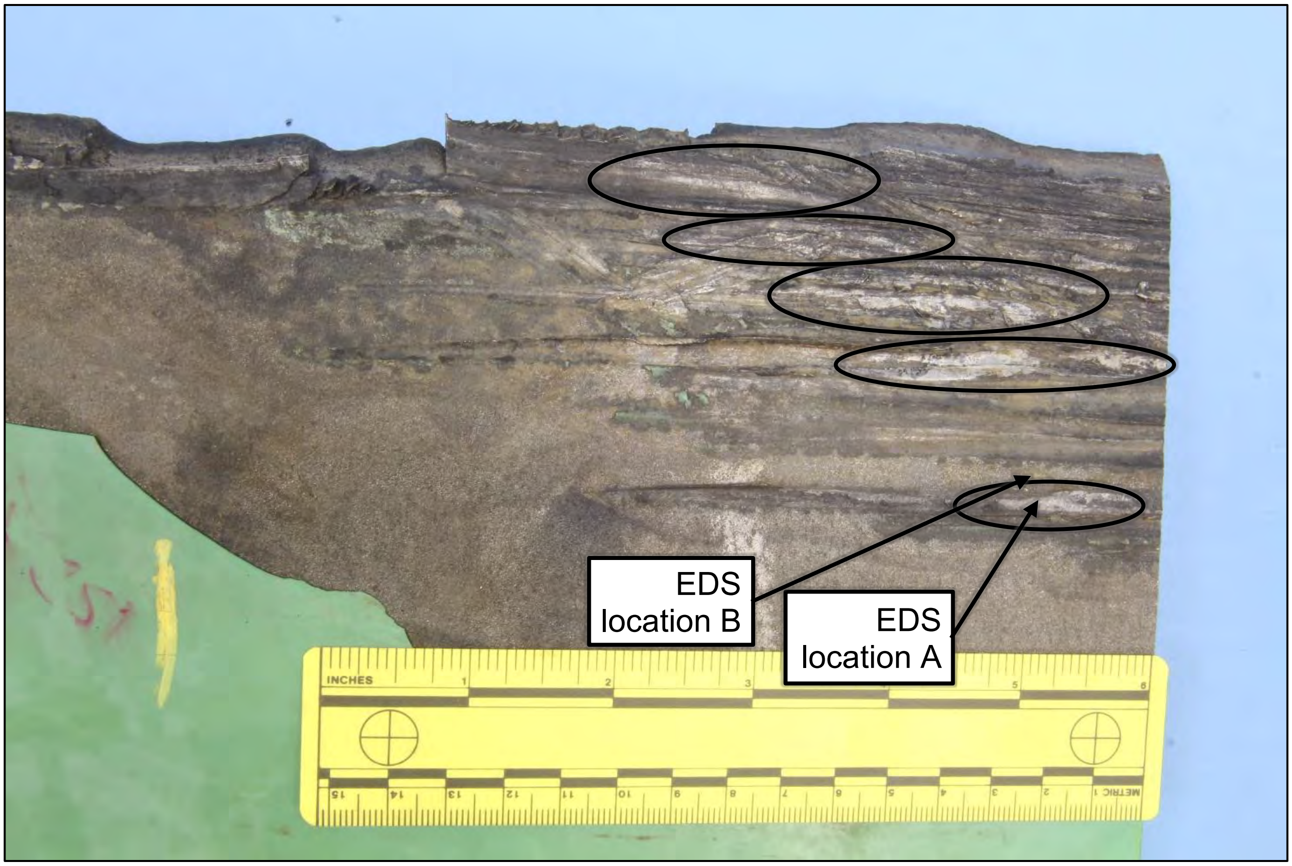

Figure 41. Circled areas on the exterior surface appeared lighter gray and more reflective consistent with less corrosion relative to the surrounding areas. These areas were all located within the sliding contact damage. EDS spectra in these areas showed a higher chromium peak than the undisturbed surfaces (see EDS spectra for locations A and B in figure 42).

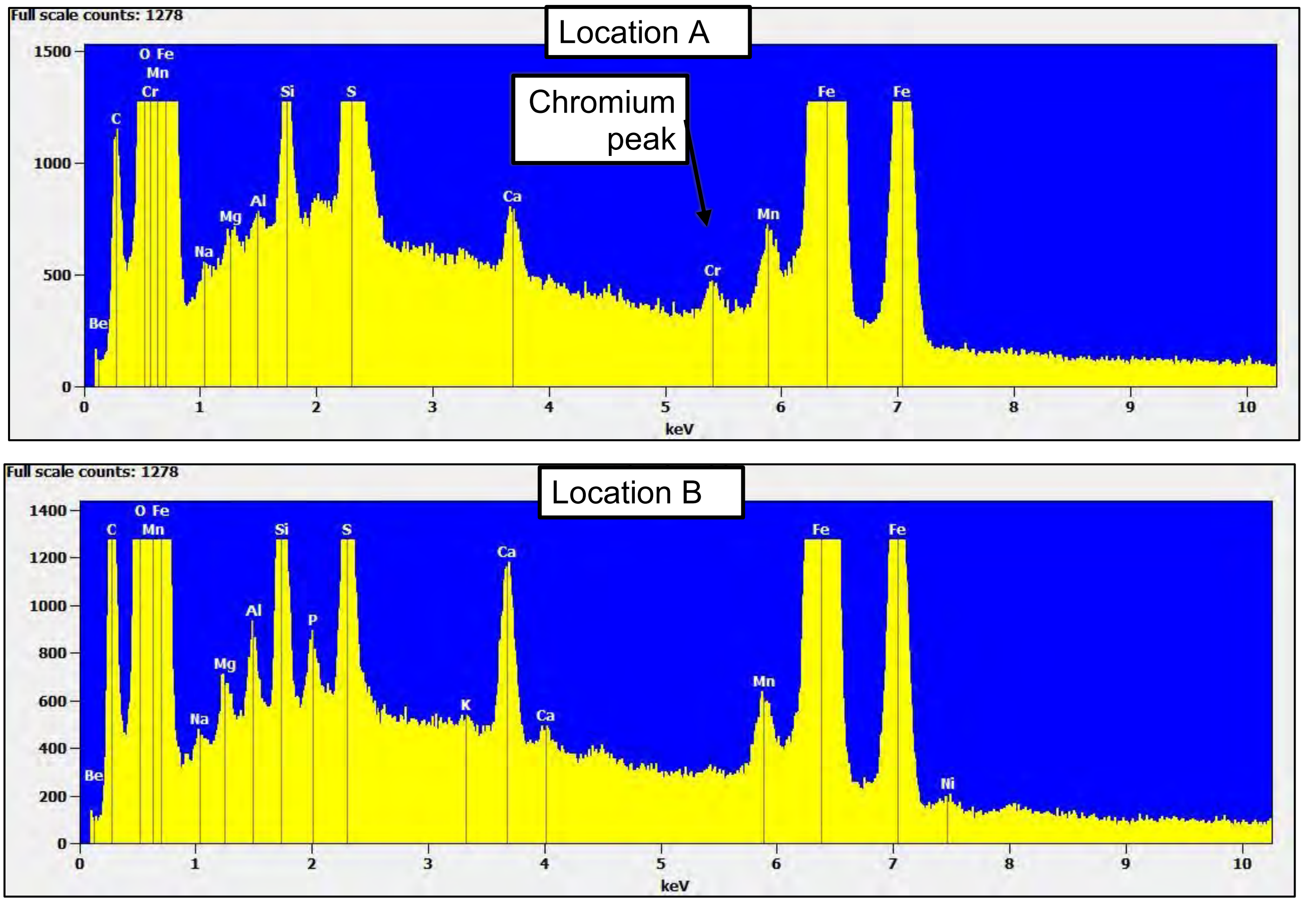

Figure 42. EDS spectra at locations indicated in figure 41. A small peak of chromium was consistently present in areas circled in figure 41 such as location A (upper spectrum) and was mostly absent in areas between sliding contact marks such as location B (lower spectrum).

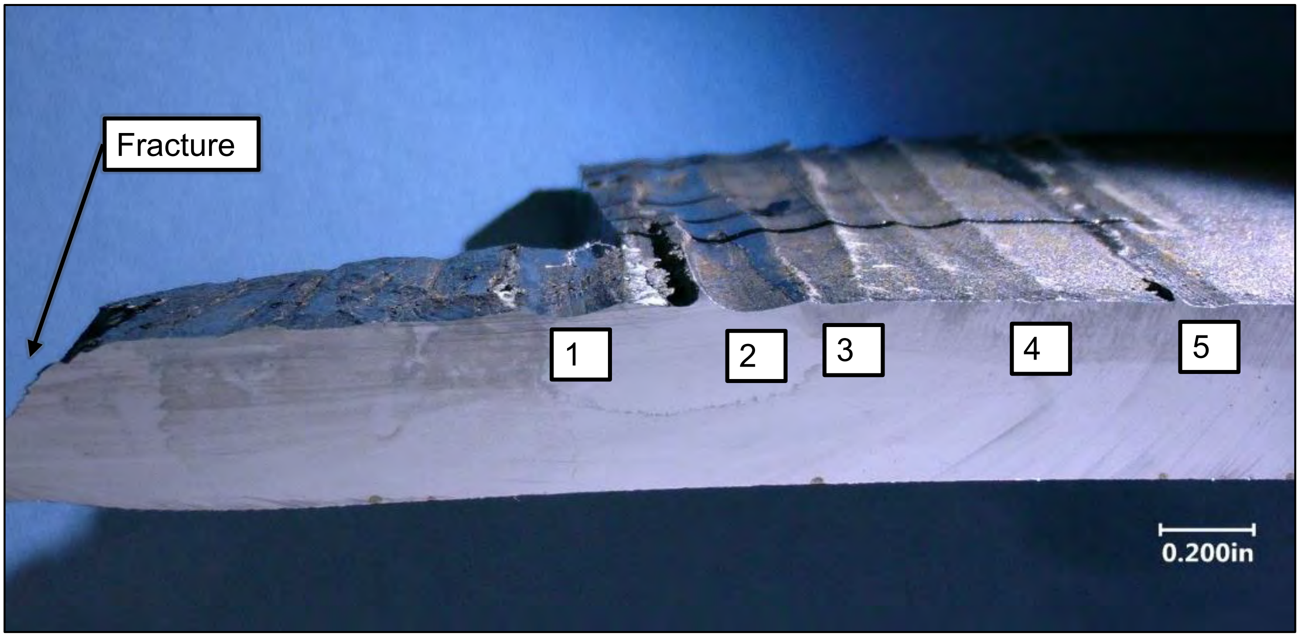

Figure 43. Optical image of the cut face of the piece adjacent to the upstream side of mount M1. Radius of curvature measurements were conducted at each of the 5 groove locations indicated.

Figure 44. Optical image of groove 1 (see figure 43). The radius of curvature was approximately 0.233 inch.

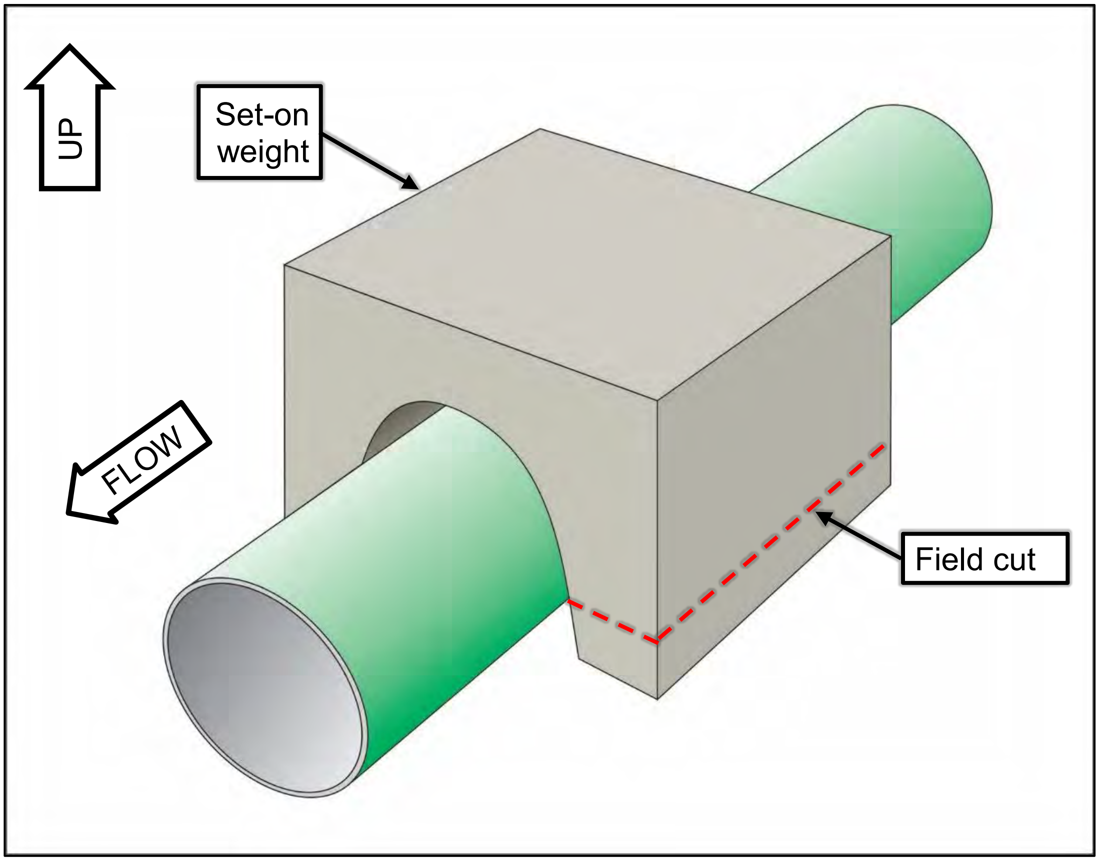

Figure 45. Schematic drawing of a concrete set-on weight installed on a pipeline. A dashed line indicates the approximate location where the weight upstream of the rupture was cut to facilitate shipment for further examination.

Figure 46. Concrete set-on piece after cleaning with soft-bristle brushes using mineral oil, acetone, and a solution of Alconox and water to remove oil and dirt from the surface. Portions of the corner between the exterior face and the lower face were also chipped away using the wood handle of the brush.

Figure 47. Another view of the cleaned set-on weight piece showing an area that was chipped away with a wood brush handle during cleaning.

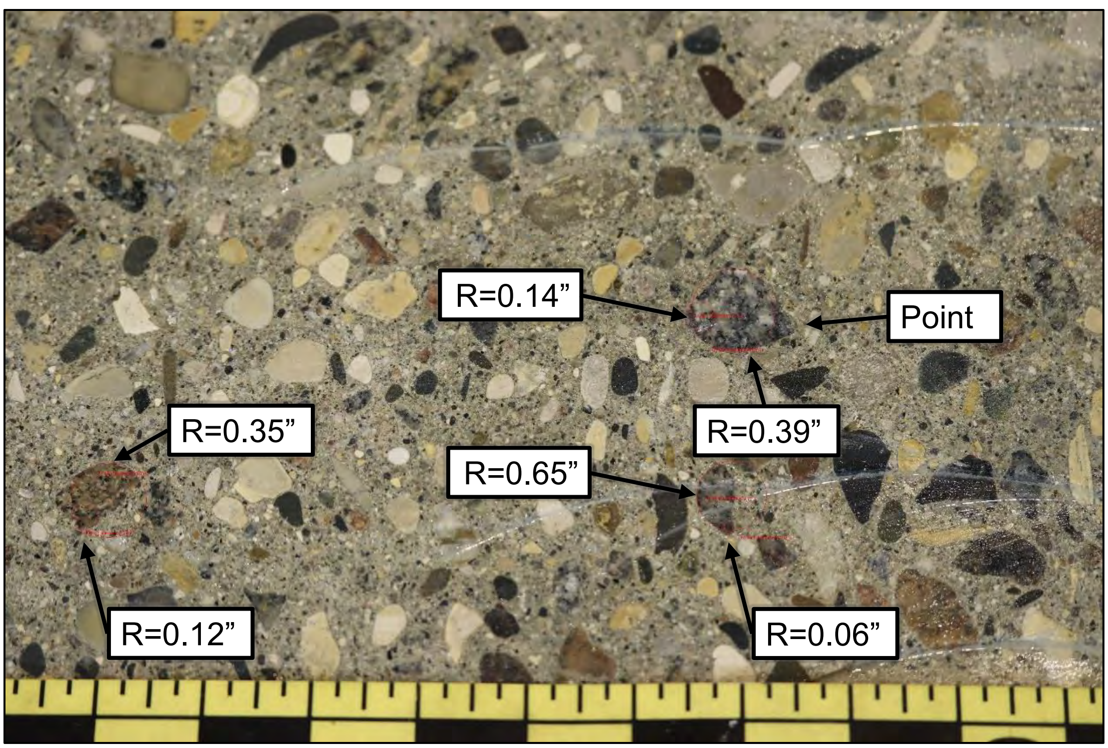

Figure 48. Cut surface of the set-on weight piece after wetting with water showing radius measurements on several pieces of quartzite plus feldspar aggregate pieces in the plane of the cut.

Figure 49. Cut face of the set-on weight piece after wetting with water. A hammer and chisel were used to chip away samples of the concrete at the corner shown.

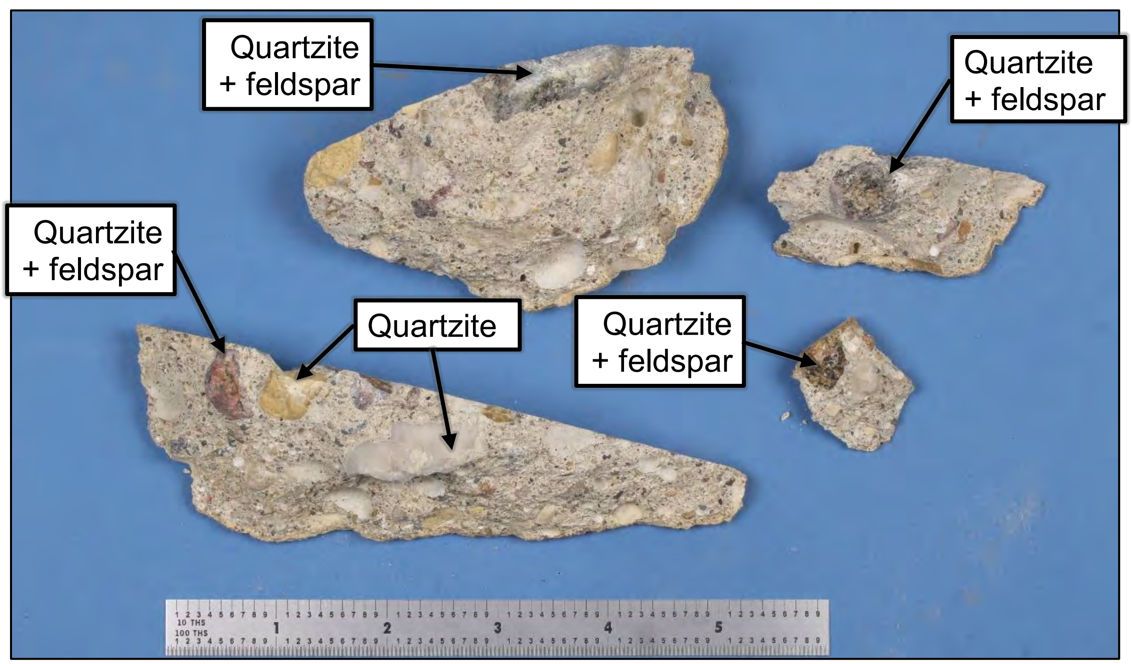

Figure 50. Several pieces of concrete chipped from the set-on weight. Some exposed pieces of aggregate identified as quartzite and quartzite plus feldspar are indicated.

D. APPENDIX A: 3D PDF OF THE RUPTURE

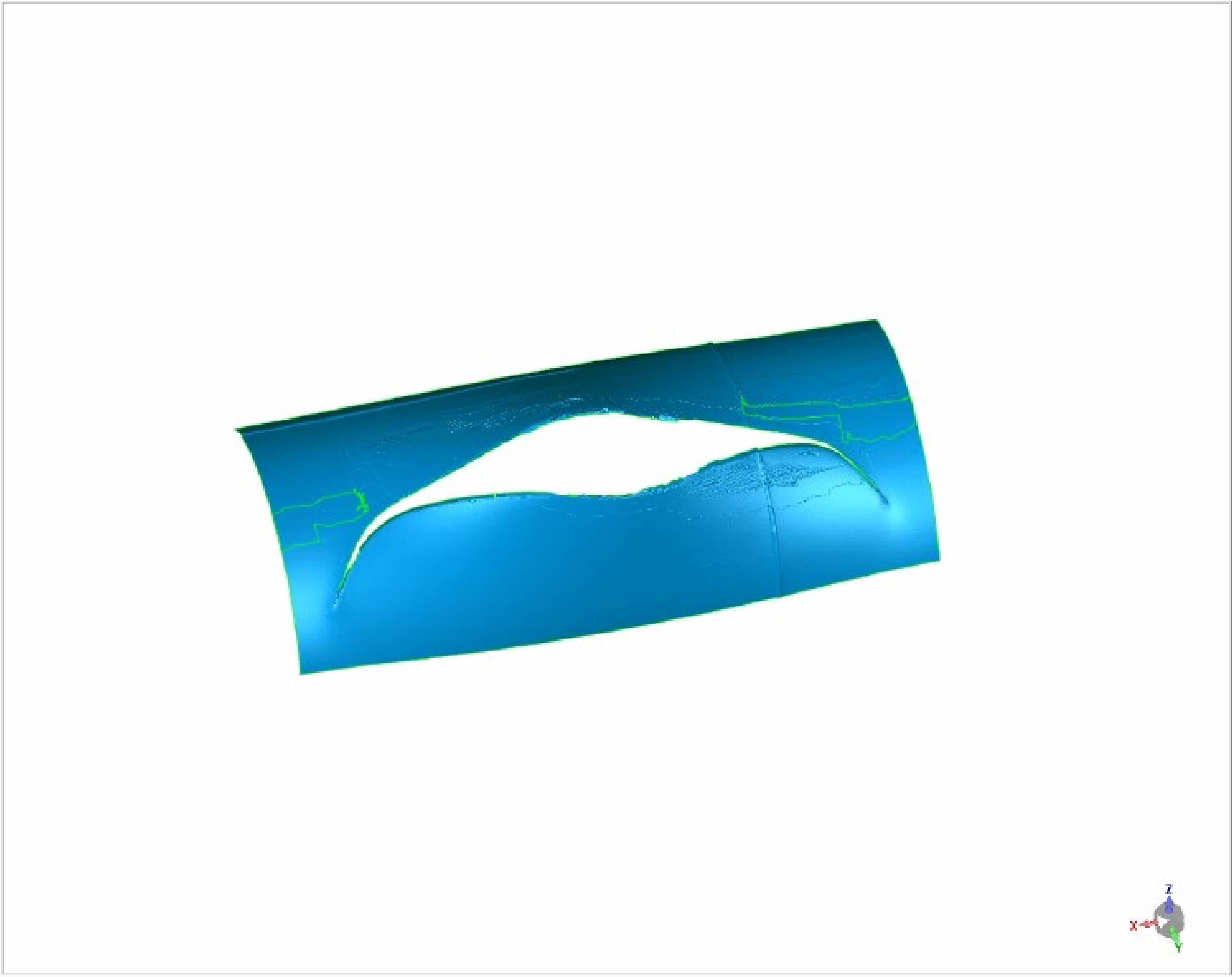

Due to file size restrictions, 3D feature has been disabled.

E. APPENDIX B: MECHANICAL TESTING AND CHEMICAL ANALYSIS REPORT

TEST REPORT

NATIONAL TRANSPORTATION SAFETY BOARD ATTENTION: MATTHEW R. FOX 490 L'ENFANT PLAZA EAST SW WASHINGTON, DC 20594	DATE: January 23, 2018 PO NO: **VERBAL** LEHIGH NO: **B-53-28** PAGE: 1 of 1

MATERIAL: API 5L GRADE X70

SAMPLE DESIGNATION: (1) SAMPLE: 16" X 18" X 0.38" SECTION REMOVED FROM A 30" OD PIPELINE, NTSB #PLD18LR001

CHEMICAL ANALYSIS (%)

Carbon	0.04
Sulfur	0.004
Manganese	1.50
Phosphorus	0.010
Silicon	0.30
Vanadium	0.03
Copper	0.21
Nickel	0.12
Chromium	0.12
Molybdenum	0.06
Aluminum	0.02
Niobium	0.07
Titanium	0.02
Boron	<0.001
Tin	0.01
Nitrogen	0.01

Results are for information only.

Procedure: *QA-CH-P-018 Rev 5 (OES)*
QA-CH-P-122 Rev 1 (Leco N)

Lehigh Testing Laboratories, Inc.

Peter M. Engelgau

Peter M. Engelgau, Principal Chemist

TEST REPORT

NATIONAL TRANSPORTATION SAFETY BOARD
ATTENTION: MATTHEW R. FOX
490 L'ENFANT PLAZA EAST SW
WASHINGTON, DC 20594

DATE: January 23, 2018

PO NO: **VERBAL**

LEHIGH NO: **B-53-28**

PAGE: 1 of 1

MATERIAL: API 5L GRADE X70
SAMPLE DESIGNATION: (1) SAMPLE: 16" X 18" X 0.38" SECTION REMOVED FROM A 30" OD PIPELINE, NTSB #PLD18LR001

MECHANICAL PROPERTIES (Per ASTM A370-16)

	A	B	C
Diameter (inches):	0.252	0.251	0.251
Area (square inches):	0.0499	0.0495	0.0495
Yield Point (ksi): 0.5% EUL:	87	87	89
Yield Strength (ksi): 0.2% offset:	87	87	89
Ultimate Tensile Strength (ksi):	95	96	97
Elongation (%) in 1":	28	31	28
Elastic Modulus:	36,011,164	32,183,620	38,089,404

Results are for information only.

Stress Strain Charts Attached.

Lehigh Testing Laboratories, Inc.

Kevin M. Sexton

Kevin M. Sexton, Mechanical Testing Technician

TEST REPORT

NATIONAL TRANSPORTATION SAFETY BOARD
ATTENTION: MATTHEW R. FOX
490 L'ENFANT PLAZA EAST SW
WASHINGTON, DC 20594

DATE: January 23, 2018

PO NO: **VERBAL**

LEHIGH NO: **B-53-28**

PAGE: 1 of 1

MATERIAL: API 5L GRADE X70
SAMPLE DESIGNATION: (1) SAMPLE: 16" X 18" X 0.38" SECTION REMOVED FROM A 30" OD PIPELINE, NTSB #PLD18LR001

IMPACT PROPERTIES (Per ASTM A370-16)

Lehigh No.	Customer ID.	Test Temp.	Imp. Energy (Ft.-Lb.)	Lat. Exp. (Mils)	Shear (%)
B-53-28-1	NTSB #PLD18LR001	212° F	112	89	100
B-53-28-2		212° F	108	86	100
B-53-28-3		212° F	111	87	100
		AVERAGE:	**110**	**87**	**100**
B-53-28-4		Room Temp 68° F	95	85	100
B-53-28-5		Room Temp 68° F	96	87	100
B-53-28-6		Room Temp 68° F	89	84	100
		AVERAGE:	**93**	**85**	**100**
B-53-28-7		23° F	83	82	100
B-53-28-8		23° F	82	81	100
B-53-28-9		23° F	79	77	100
		AVERAGE:	**81**	**80**	**100**

Specimen Size: 6.7mm X 10mm

Results are for information only.

Lehigh Testing Laboratories, Inc.

Kenneth M. Petito

Kenneth M. Petito, Supvr., Mechanical Testing

TEST REPORT

NATIONAL TRANSPORTATION SAFETY BOARD
ATTENTION: MATTHEW R. FOX
490 L'ENFANT PLAZA EAST SW
WASHINGTON, DC 20594

DATE: January 23, 2018

PO NO: **VERBAL**

LEHIGH NO: **B-53-28**

PAGE: 1 of 1

MATERIAL: API 5L GRADE X70
SAMPLE DESIGNATION: (1) SAMPLE: 16" X 18" X 0.38" SECTION REMOVED FROM A 30" OD PIPELINE, NTSB #PLD18LR001

IMPACT PROPERTIES (Per ASTM A370-16)

Lehigh No.	Customer ID.	Test Temp.	Imp. Energy (Ft.-Lb.)	Lat. Exp. (Mils)	Shear (%)
B-53-28-10	NTSB #PLD18LR001	-50° F	76	74	100
B-53-28-11		-50° F	73	72	100
B-53-28-12		-50° F	72	70	100
		AVERAGE:	**74**	**72**	**100**
B-53-28-13		-100° F	64	63	100
B-53-28-14		-100° F	67	66	100
B-53-28-15		-100° F	64	62	100
		AVERAGE:	**65**	**64**	**100**

Specimen Size: 6.7mm X 10mm

Results are for information only.

Lehigh Testing Laboratories, Inc.

Kenneth M. Petito

Kenneth M. Petito, Supvr., Mechanical Testing

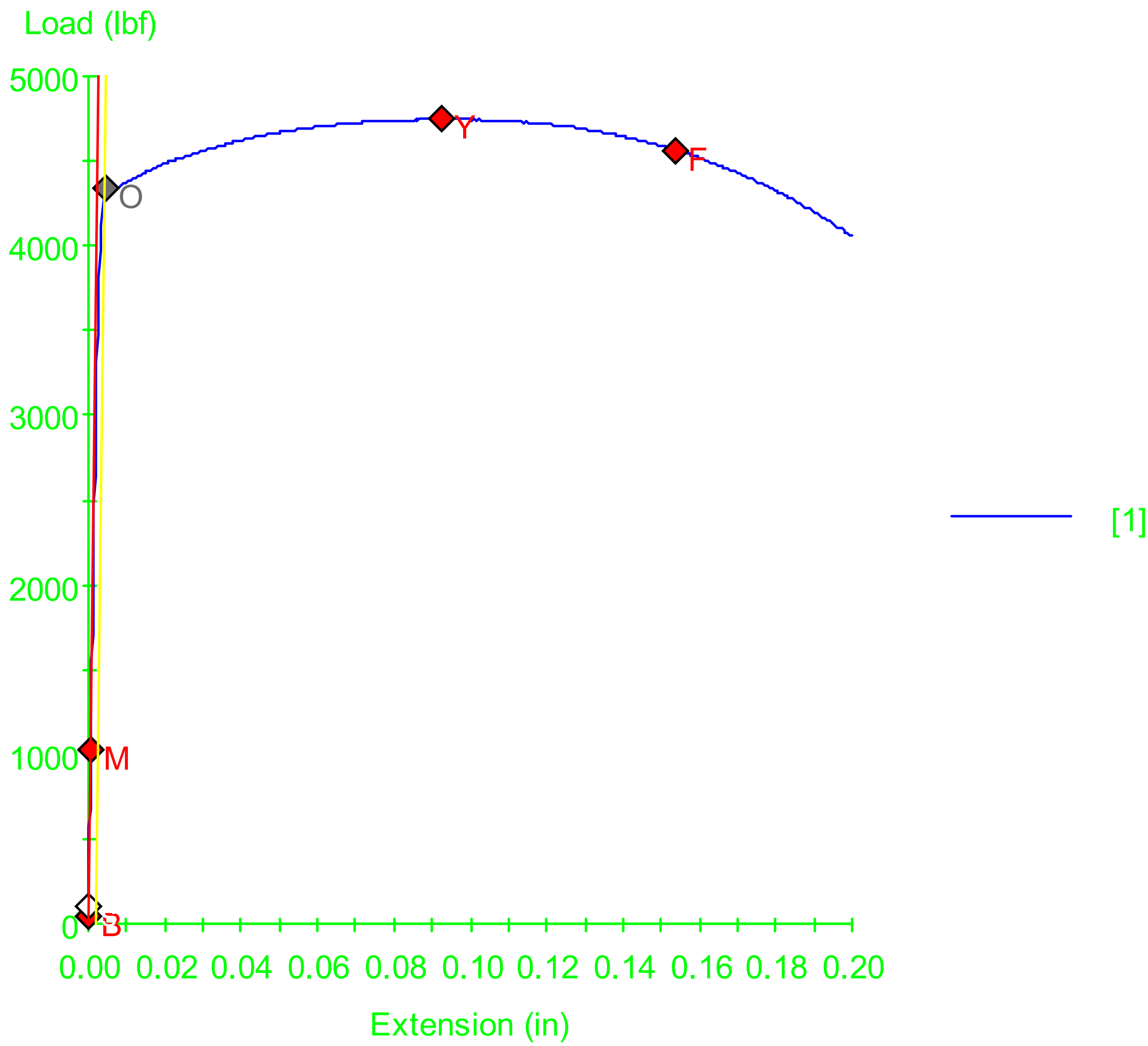
Load (lbf)
5000
4000
3000
2000
1000
0
O
Y
F
M
B
0.00 0.02 0.04 0.06 0.08 0.10 0.12 0.14 0.16 0.18 0.20
Extension (in)
[1]

"A"

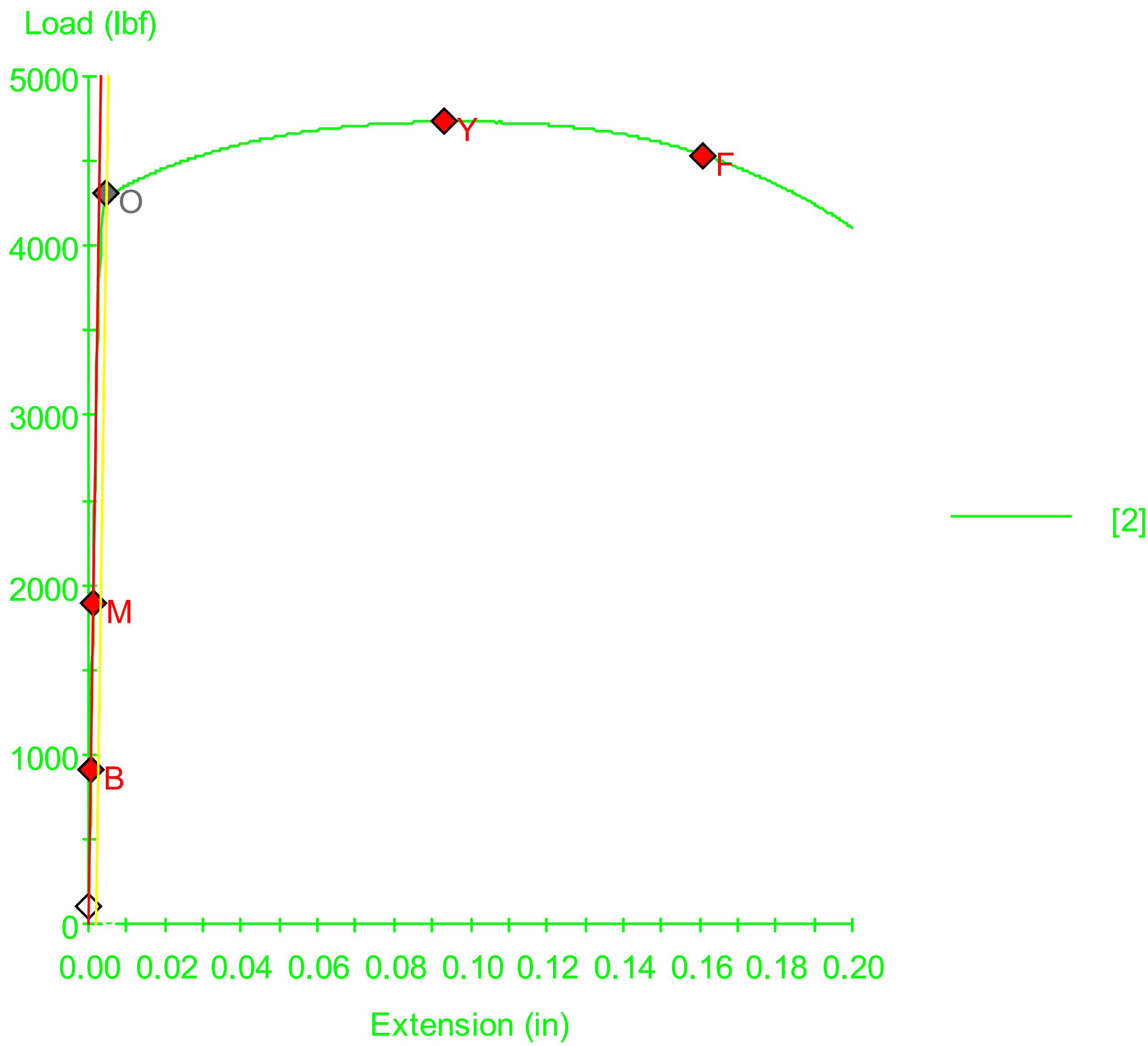

Load (lbf)
5000
4000
3000
2000
1000
0
0.00
0.02
0.04
0.06
0.08
0.10
0.12
0.14
0.16
0.18
0.20
Extension (in)
Y
F
O
M
B
[2]

"B"

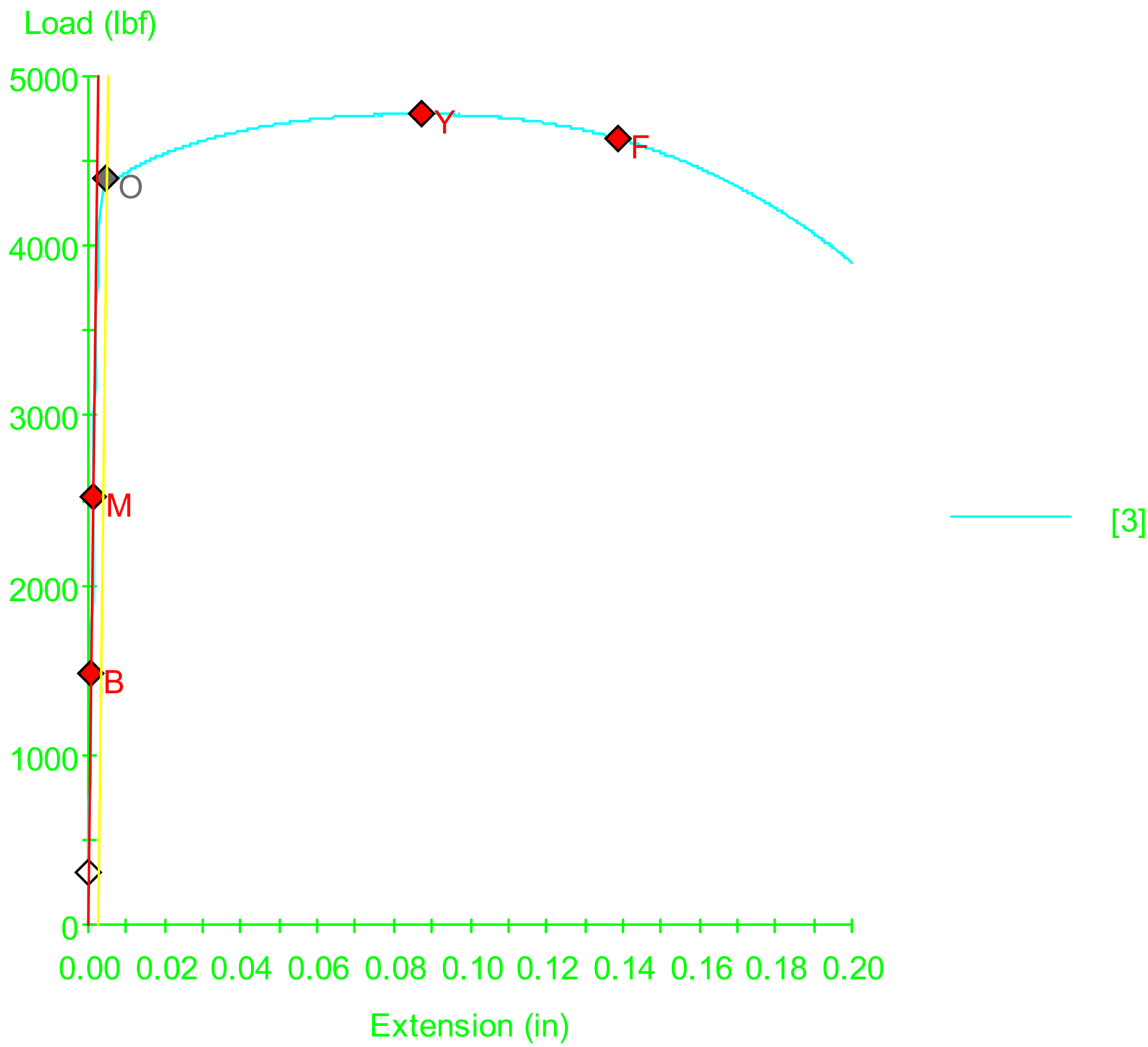
Load (lbf)
5000
4000
3000
2000
1000
0
O
Y
F
M
B
0.00 0.02 0.04 0.06 0.08 0.10 0.12 0.14 0.16 0.18 0.20
Extension (in)
[3]

"C"